

# Mode of life and hydrostatic stability of orthoconic ectocochleate cephalopods: Hydrodynamic analyses of restoring moments from 3D printed, neutrally buoyant models

DAVID J. PETERMAN, CHARLES N. CIAMPAGLIO, RYAN C. SHELL,  
and MARGARET M. YACOBUCCI



Peterman, D.J., Ciampaglio, C.N., Shell, R.C., and Yacobucci, M.M. 2019. Mode of life and hydrostatic stability of orthoconic ectocochleate cephalopods: Hydrodynamic analyses of restoring moments from 3D printed, neutrally buoyant models. *Acta Palaeontologica Polonica* 64 (3): 441–460.

Theoretical 3D models were digitally reconstructed from a phragmocone section of *Baculites compressus* in order to investigate the hydrostatic properties of the orthoconic morphotype. These virtual models all had the capacity for neutral buoyancy (or nearly so) and were highly stable with vertical *syn vivo* orientations. Body chamber lengths exceeding approximately 40% of the shell length cause buoyancy to become negative with the given modeled proportions. The distribution of cameral liquid within the phragmocone does not change orientation and only slightly influences hydrostatic stability. The mass of cameral liquid required to completely reduce stability, permitting a non-vertical static orientation, would cause the living cephalopod to become negatively buoyant. A concave dorsum does not significantly change the mass distribution and results in a 5° dorsal rotation of the aperture from vertical. The restoring moments acting to return neutrally buoyant objects to their equilibrium position were investigated using 3D-printed models of *Nautilus pompilius* and *Baculites compressus* with theoretically equal masses and hydrostatic stabilities to their virtual counterparts. The *N. pompilius* behaved as an underdamped harmonic oscillator during restoration due to its low hydrostatic stability and drag relative to the *B. compressus* model. In contrast, the *B. compressus* model more quickly returns to its equilibrium position without oscillating (overdamped system). The thrust required to overcome such a large restoring moment was explored using several extant cephalopod analogues. Significant angles of displacement were only achieved with coleoid-like thrusts, which were unrealistically high despite the probable similarities in their locomotor design. These maximum bursts of thrust may have been too energetically expensive and would preclude an unusual form of locomotion in a non-vertical orientation. These results suggest baculitids and other orthocones with similar hydrostatic stabilities probably lived a nektonic to quasilanktic mode of life with a primarily vertical orientation and mobility.

**Key words:** Cephalopoda, Ammonoidea, *Baculites*, 3D imaging, 3D printing, hydrostatics, buoyancy, Cretaceous.

David J. Peterman [peterman.10@wright.edu] and Ryan C. Shell [shell.24@wright.edu], Department of Earth and Environmental Sciences, Wright State University, 3640 Colonel Glenn Hwy, Dayton, OH 45435, USA.

Charles N. Ciampaglio [chuck.ciampaglio@wright.edu], Department of Science and Mathematics, Wright State University Lake Campus, Dwyer Hall 219, 7600 Lake Campus Dr., Celina, OH 45822, USA.

Margaret M. Yacobucci [mmyacob@bgsu.edu], Department of Geology, Bowling Green State University, 190 Overman Hall, Bowling Green, Ohio 43403, USA.

Received 9 January 2019, accepted 11 April 2019, available online 30 July 2019.

Copyright © 2019 D.J. Peterman et al. This is an open-access article distributed under the terms of the Creative Commons Attribution License (for details please see <http://creativecommons.org/licenses/by/4.0/>), which permits unrestricted use, distribution, and reproduction in any medium, provided the original author and source are credited.

## Introduction

*Function of ectocochleate cephalopod shells and their hydrostatics.*—The conch of ectocochleate (externally-shelled) cephalopods consists of a body chamber that was inhabited by the living animal and a phragmocone that is di-

vided by septa into a series of progressively larger chambers (camerae) during growth. The soft body and mineralized shell are denser than seawater and are negatively buoyant while the phragmocone is positively buoyant due to some fraction of gas in its chambers. The phragmocone allows the cephalopod to achieve neutral buoyancy and functions as a passive gas float by regulating the weight and bulk

density of the cephalopod. Neutral buoyancy is achieved when the total mass of the organism is equal to the mass of the displaced seawater. The *syn vivo* static orientation of a neutrally buoyant object occurs when the centers of buoyancy and mass are aligned vertically. Hydrostatic stability is determined by the degree of separation between these two centers (Okamoto 1996). A larger separation between the centers of buoyancy and mass relative to their weight will result in a larger restoring moment: a torque resulting from the downward acceleration of gravity acting on the center of mass and an upward buoyant force acting on the center of buoyancy. After displacing the centers of mass and buoyancy from a vertical alignment, this restoring moment returns the neutrally buoyant cephalopod to its equilibrium position. The rocking behavior of extant nautilids during locomotion reflects this hydrodynamic restoration after each jet pulse (Chamberlain 1981; Jacobs and Landman 1993). The manner in which this restoring moment acted upon extinct taxa during life is largely unknown, especially for non-planispiral morphotypes. Therefore, it is crucial to investigate the hydrostatic and hydrodynamic properties of different ectocochleate cephalopod morphotypes to better understand their specific modes of life and life habits.

We constructed several virtual 3D models of the Late Cretaceous heteromorph ammonoid *Baculites compressus* Say, 1820 to investigate the constraints and sensitivities on the hydrostatic properties of the straight-shelled (orthoconic) morphotype. This approach included calculating the liquid to gas ratio necessary for a neutrally buoyant condition, as well as the volume of the shell, camerae, and soft body. These properties were used to compute the *syn vivo* orientation and hydrostatic stability of this species, which provide a better understanding of the orthoconic morphotype and baculitid mode of life. The restoring moments acting on a baculite displaced from its equilibrium position were also experimentally assessed with 3D printed models that have theoretically equal mass distributions and buoyancy to the virtual 3D models.

*Previous studies of baculite hydrostatics and mode of life.*—The study of the geometry, buoyancy, and hydrostatics of ammonoids was pioneered by Moseley (1838) and Trueman (1941) in work that promoted a better understanding of ammonoid modes of life and led to many theoretical and empirical studies on these subjects (Raup and Chamberlain 1967; Saunders and Shapiro 1986; Shigeta 1993; Tanabe et al. 1995; Okamoto 1996; Kröger 2002; Hoffmann et al. 2014, 2015, 2018; Tajika et al. 2015a, b; Lemanis et al. 2015; Naglik et al. 2015a, Peterman and Barton 2017; Peterman et al. 2018, 2019; Peterman and Ciampaglio 2018). Trueman (1941) suggested that baculitids, as orthoconic heteromorphs would have been stably oriented with their aperture inclined downwards at rest due to the positive buoyancy of earlier chambers. This same orientation is also present in orthoconic nautiloids, endoceratoids, and actinoceratoids (Trueman 1941; Klinger 1980; Tsujita and Westermann 1998; Peterman et al. 2018), which have high hydrostatic

stability in groups not possessing significant masses of cameral or endosiphuncular deposits (Peterman et al. 2019). The orthoconic morphotype of ectocochleate cephalopods has high hydrostatic stability relative to other morphotypes because its mass distribution is moved in a beeline fashion away from the center of buoyancy. Thus, a highly-stable, vertical orientation for orthoconic ectocochleates without cameral or endosiphuncular deposits has been commonly accepted (Reyment 1973; Ward 1976; Westermann 1977, 1996, 2013; Klinger 1980; Batt 1989; Peterman et al. 2018, 2019).

While much evidence suggests that a highly-stable, vertical, static orientation is likely for orthocones, this interpretation is not without its caveats. Westermann (1977, 1996, 2013), Klinger (1980), and Tsujita and Westermann (1998) suggested that orthoconic ammonoids could deviate from this vertical posture by flooding the adapical portion of their phragmocone to act as a liquid counterweight. Westermann (2013) experimented on orthocone hydrostatics by creating several 2D models with neutral buoyancy. These models consist of several regions partitioned into cameral gas, cameral liquid, and the body chamber. Westermann (2013) found that models with adapically placed gas and flooded chambers directly behind the body had stable vertical orientations. However, placing the same proportion of cameral liquid adapically was found to reduce stability enough to permit horizontal swimming. Westermann (2013) also attempted to replicate the concave dorsum similar to *Baculites grandis* Hall and Meek, 1854 by creating a “quadripartite” model with adapical and adoral emptied chambers and a flooded portion in between. According to his model, a somewhat stable horizontal orientation was achieved without rolling (keeping the venter oriented downwards). A physical experiment was performed in his study where *B. grandis* was modeled with plexiglass, styrofoam, and various internal iron weights and which experienced a horizontal orientation when neutrally buoyant.

A non-vertical (sub-horizontal) orientation was inferred for the baculitid *Sciponoceras* sp. (Hauschke et al. 2011) by the orientation of a cirripede epizoan on the venter of the shell. The authors also suggested a forward direction of locomotion for this baculitid because the cirripede grew from the venter and slightly rotated the feeding apparatus towards the aperture throughout growth. This epizoan behavior is also recorded for planispiral ectocochleate cephalopods including other ammonoids and even the extant *Nautilus* (Keupp et al. 1999; Seilacher and Keupp 2000; Hoffmann and Keupp 2015; Seilacher and Gishlick 2015; Naglik et al. 2015b).

The depth range of baculitids (including *B. compressus*) in the Western Interior Seaway of the United States may have been around 50–100 m based on isotopic analyses (Fatherree et al. 1998; Lukeneder et al. 2010; Landman and Klofak 2012; Henderson and Price 2012; Lukeneder 2015; Landman et al. 2018). Additionally, a demersal habitat is inferred from these analyses due to their isotopic similarity

with the benthos (Sessa et al. 2018; Landman et al. 2018), which suggests that these baculitids may have lived within a few meters from the sea bottom. Ontogenetic sampling of baculites from methane seeps reveals they probably did not laterally migrate over long distances and spent the majority of their lives at or nearby these sites (Landman et al. 2018).

Information about the baculitid diet can be inferred by the morphology of the buccal mass. Kruta et al. (2011) reported on a buccal mass of a baculite revealed by synchrotron X-ray microtomography that had remains of possible prey items including pelagic isopods and possibly a larval gastropod. The morphology of the baculitid buccal mass along with the remains of potential prey suggests that they fed on small organisms in the water column (Kruta et al. 2011). This interpretation is reinforced by Klug et al. (2012), who also suggest a planktotrophic feeding habit based on several well-preserved baculitids.

*Three-dimensional modeling of ectocochleate cephalopods.*—Recently, accurate hydrostatic analyses have been improved by tomographic techniques. The application of computed tomography (CT) can yield 3D models with excellent precision to aid in morphometry (Hoffmann et al. 2014; Lemanis et al. 2015; Tajika et al. 2015b) and the approach has been used for hydrostatic calculations, including the conditions for neutral buoyancy (Hoffmann et al. 2014, 2015, 2018; Lemanis et al. 2015). However, low contrasts in physical properties (X-ray attenuation, etc.) between the matrix and/or mineral growth inside chambers and the fossil shell can yield problems in imaging the fossil anatomy, as can averaging of densities of different materials within each voxel (the partial volume effect; see Hoffmann et al. 2014). The ideal scenario involves well-preserved specimens with hollow chambers, or in the case of Inoue and Kondo (2016), chamber casts surrounded by a void after shell dissolution. The reconstruction of ammonites with complex septal frilling is especially difficult where mineral growth covers the internal shell and/or septa and distorts higher-order folds. When the conditions are adequate for ideal 3D reconstructions, these models can be used to compute the hydrostatic properties from the volumes, and therefore mass, of the materials occupying the camerae, soft body, shell, and any other feature with a unique density. These morphometrics can be then used to compute buoyancy, *syn vivo* orientation, and stability. Serial grinding tomography is also a valuable tool for constructing models to be used in morphometry and hydrostatic calculations (Tajika et al. 2015a, b; Naglik et al. 2015a, 2016). These techniques can produce 3D models from processing many successive slices through an object. Of course, this method is invasive and causes complete destruction of the specimen. It is also susceptible to the partial volume effect and other discrepancies (Hoffmann et al. 2014).

While tomographic techniques can produce accurate 3D models of cephalopod shells, they rely on ideal specimens that are complete, undeformed, and have appropriate contrasts (either optically or by attenuation factor) between the

shell and its surroundings. Theoretical 3D models for virtual paleontology are a necessary alternative to tomographic modeling for rare species or specimens that seldom preserve in an adequate manner for 3D imaging. Such models can be generated by imaging and reconstructing multiple fragmentary specimens or replicating real pieces until the whole specimen is virtually reconstructed. Such reconstructions can be performed with the use of photogrammetry in the absence of access to tomographic equipment or expensive surface scanners. Photogrammetry can be used to scan the exterior of a specimen by generating a 3D mesh from a series of overlapping photographs (Sutton et al. 2014). This method has been more recently used in paleontology (Petti et al. 2008; Falkingham 2012; Knauss and Yacobucci 2014; Fau et al. 2016), and can yield 3D models of comparable resolution to high quality surface scanners (Fau et al. 2016). This cheap and portable technique (Cunningham et al. 2014) can be suitable to produce theoretical models of ectocochleate cephalopod shells for the computation of their hydrostatic properties (Peterman and Barton 2017; Peterman and Ciampaglio 2018).

*Institutional abbreviations.*—WSU, Department of Earth and Environmental Sciences, Wright State University, Dayton, Ohio, USA.

*Other abbreviations.*—BCL, body chamber length; L, length; PLA, polyactic acid; St, hydrostatic stability.

## Material and methods

*Modelled specimens.*—Orthoconic (straight-shelled) cephalopods (e.g., nautiloids, baculitids, etc.) are rarely found complete because long, slender, hollow shells are subject to several taphonomic processes that result in disarticulation and alteration. A baculite was chosen for the current study because specimens are common and excellently preserved in concretions within the Upper Cretaceous Pierre Shale in the United States, Western Interior. Such specimens exhibit largely unaltered shell material that is required to define shell and septum thicknesses and ultimately the volume for theoretical virtual models. Fragmentary specimens of the late Campanian baculite species *Baculites compressus* were used in this study to create the 3D models and measure shell and septal thicknesses. These specimens are currently housed at WSU.

*Virtual model generation.*—The virtual 3D model of the extant *Nautilus pompilius* from Peterman et al. (2019: fig. 2.5) was used in the current study to serve as a reference for the hydrostatic experiments of the orthoconic *Baculites compressus*. This model also served as an assessment of the experimental modeling techniques used in this study. The *Nautilus pompilius* model, although isometric, was found to have very similar hydrostatic properties to a model generated from a CT scanned specimen (Hoffmann et al. 2014;

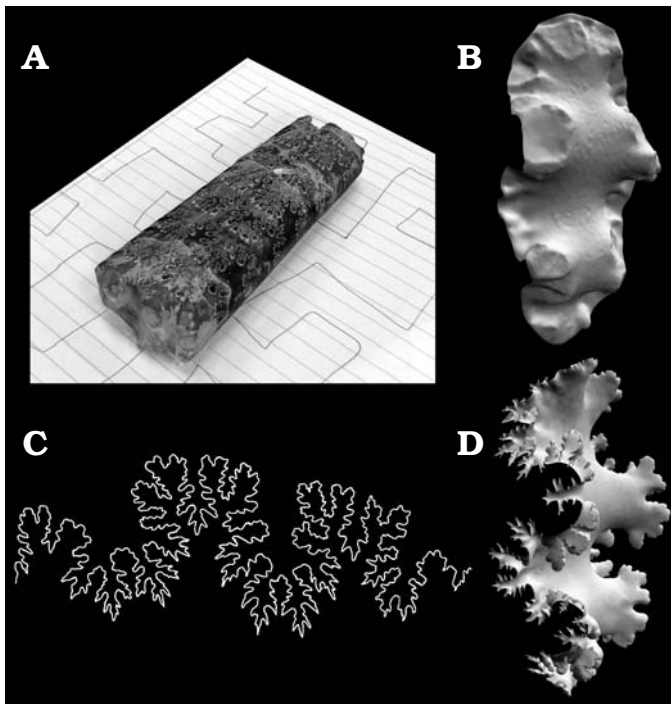


Fig. 1. Three-dimensional reconstruction of a fragmentary baculite *Baculites compressus* Say, 1820 (WSU-1400) from the late Campanian Pierre Shale of Meade County, South Dakota. **A.** Model of a fragmentary specimen generated by photogrammetry with the software (3DF Zephyr). **B.** Broken septum isolated from the photogrammetry model. **C.** Suture pattern. **D.** Complete septum created by reconstructing the higher-order frilling with the suture pattern as a template.

Lemanis et al. 2015, 2016), especially in terms of hydrostatic stability (Peterman et al. 2019).

Several theoretical 3D models were digitally reconstructed from a fragmentary specimen of *Baculites compressus* (WSU-1400). A 3D shapefile of this specimen was created with 3DF Zephyr (3DFlow 2018) photogrammetry software (Fig. 1A). This produces a tessellated 3D mesh (in .stl format) from a series of photographs taken around the object (~50 for optimum coverage). The digitized specimen consists of a section of a phragmocone with eight septa. An exposed septum at the adoral edge of the specimen (Fig. 1B) was used as a base to reconstruct the entire septum. The suture line (Fig. 1C) was used as a template to reconstruct the higher order frilling. An array of sculpting tools in Meshmixer (Autodesk Inc. 2017a) was used in order to manually reconstruct the frilled margins (Fig. 1D). The smoothing tool in Meshmixer (Autodesk Inc. 2017a) was used to approximate the curvature of the septum between the frilled margins and preserved first and second order folds. All reconstruction was performed on only half of the model. Meshmixer's mirror utility was used at the end of processing in order to minimize errors in reconstruction by replicating the reconstructed portion of the model about the sagittal plane.

After reconstructing a single septum, it was then duplicated and placed inside the segment of shell that was originally scanned. The magnetize tool in Meshmixer (Autodesk

Inc. 2017a) was used to seal the space between the septa and the shell while simultaneously smoothing the model. The septal spacing was relatively constant and was achieved by placing the farthest-reaching folioles tangential to the farthest-reaching lobules from the previous (adoral) septum. This yielded a single septate section of shell which was then duplicated in order to recreate the entire phragmocone of the baculite using the degree of taper from the scanned fragment. The living chamber was constructed by using the originally scanned shell fragment with the same degree of taper.

Measurements of shell and septum thickness were made using digital calipers on well-preserved specimens (WSU-1400, WSU-1401, and WSU-1450). Exponential curves (Fig. 2) were used to estimate shell and septum thickness in the model corresponding to whorl heights (Wh). The 3D computer graphics software, Blender, was used to define thickness of the model. This process, called extrusion, was performed with positive offset on the external shell segments. These segments were then sealed together and smoothed in Meshmixer (Autodesk Inc. 2017a) in order to recreate an extruded thickness gradient similar to the actual shell of an adult *Baculites compressus* (Fig. 2). The 83 septa were individually extruded in Blender with zero offset and combined with the extruded shell to create a complete shell model (Fig. 3A). The length of the body chamber was reconstructed at 40% and 33% of the total length of the baculite in order to compare the hydrostatics between the upper and lower limits of the "mesodome" body chamber ratio (Westermann 2013).

The soft body was reconstructed by deleting the external wall of the baculite shell mesh and isolating the living chamber. This represents the interface between mineralized shell and the soft body. The normals of the faces were inverted (which denote the exterior direction of the mesh) to produce a mesh that appropriately has its normals pointing outwards. The soft body, which resembles the baculitid reconstruction

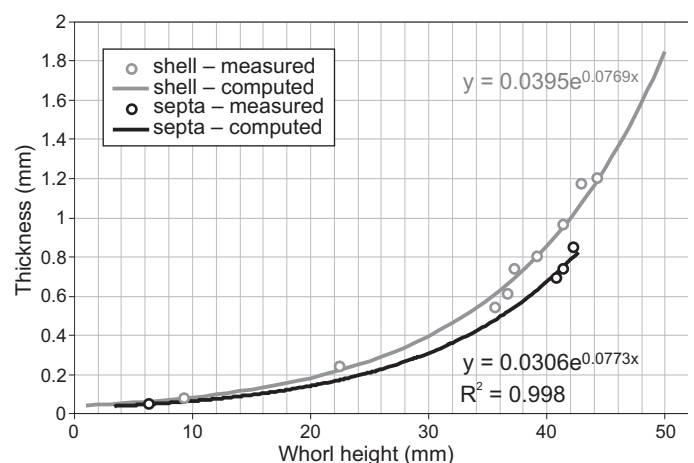


Fig. 2. Shell and septum thickness measured from three specimens of *Baculites compressus* (WSU-1400, WSU-1401, and WSU-1405). Exponential curves were fit to these points to define thickness for the full 3D model as a function of whorl height.

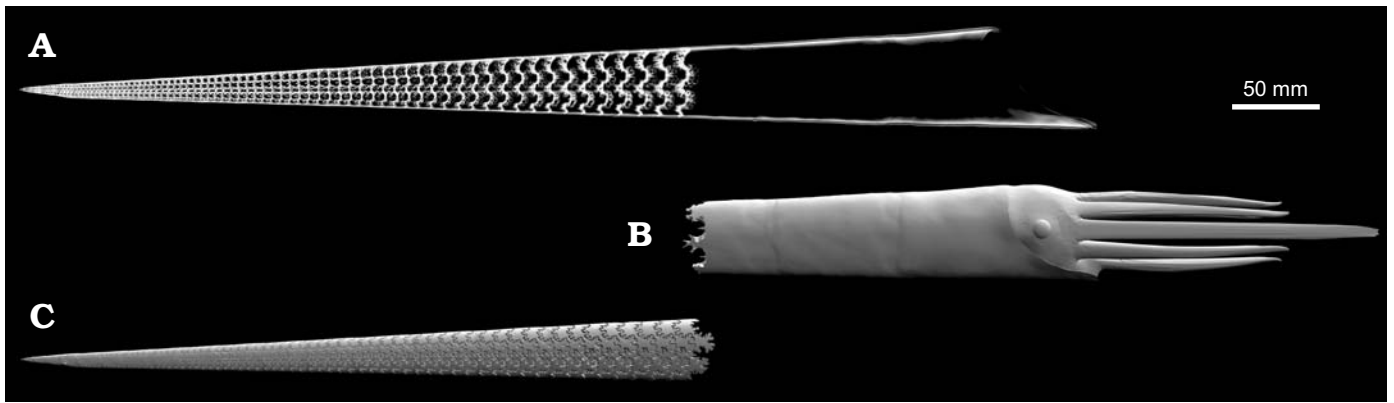


Fig. 3. Full 3D model of *Baculites compressus* with model components. A. Complete, digitally-reconstructed shell rendered in X-ray view to show internal structure. B. Three-dimensional model the soft body. C. Three-dimensional model of the cameral volumes within the phragmocone.

of Klug et al. (2012), was then constructed and shaped to fit inside the living chamber (Fig. 3B). Each camera was reconstructed in a similar manner to the soft body. The exterior mesh of the phragmocone was deleted and the internal interfaces were isolated and inverted. This allowed the reconstruction of all camerae (Fig. 3C) and for each of their volumes to be calculated. Each model had to be repaired using Autodesk Netfabb (Autodesk Inc. 2017b) to remove non-manifold elements and other mesh errors in order to calculate geometric measurements. All volumes and centers of mass were then calculated with MeshLab (Cignoni and Ranzuglia 2014).

*Hydrostatic calculations.*—Hydrostatic calculations herein largely follow the methods of Peterman et al. (2019). The proportion of cameral gas and cameral liquid to produce a neutrally buoyant condition was calculated for each model using a modification of Archimedes principle:

$$m_{sb} + m_{sh} + m_{cl} + m_{cg} = m_{wd} \tag{1}$$

where  $m_{sb}$  is the mass of the soft body,  $m_{sh}$  is the mass of the shell,  $m_{cl}$  is the mass of cameral liquid,  $m_{cg}$  is the mass of cameral gas, and  $m_{wd}$  is the total mass of water displaced.

The ratio of the volume of cameral gas to total cameral volume ( $\Phi$ ) is found by setting Equation 1 in terms of density and volume then solving for  $\Phi$ :

$$\Phi = \frac{\left(\frac{V_{wd}\rho_{wd} - V_{sb}\rho_{sb} - V_{sh}\rho_{sh}}{V_{ct}}\right) - (\rho_{cl})}{(\rho_{cg} - \rho_{cl})} \tag{2}$$

where  $V_{wd}$  and  $\rho_{wd}$  are the volume and density of the water displaced by the entire model,  $V_{sb}$  and  $\rho_{sb}$  are the volume and density of the soft body,  $V_{sh}$  and  $\rho_{sh}$  are the volume and density of the shell,  $\rho_{cl}$  is the density of cameral liquid,  $\rho_{cg}$  is the density of cameral gas, and  $V_{ct}$  is the total volume of all camerae. A soft body density of 1.065 g/cm<sup>3</sup> is adopted from Westermann (2013) and is assumed here to uniformly fill the living chamber (Fig. 3B). A shell density of 2.62 g/cm<sup>3</sup> is also commonly accepted (Reyment 1958; Okamoto 1996; Klug and Hoffmann 2015). The density of cameral liquid is assumed to be equal to that of seawater (1.025 g/cm<sup>3</sup>;

Greenwald and Ward 1987). The density of cameral gas is negligible, but set here for calculations as 0.001 g/cm<sup>3</sup>.

The volumes of cameral gas and liquid necessary for neutral buoyancy were then modeled by splitting the shapefile containing all of the modeled camerae (Fig. 3C) into their appropriate gas and liquid fractions. These models do not include the pellicle or liquid retained via capillary forces. They also do not include the siphuncle, a feature with a probably negligible mass relative to the total organismal mass (Lemanis et al. 2015).

The models of the shell, soft body, cameral gas, and cameral liquid each have a density-weighted influence on the mass distribution of the living baculite due to their differences in density and geometry. The total center of mass from these models of differing densities was calculated with the formula:

$$M = \frac{\sum(L \cdot m_o)}{\sum m_o} \tag{3}$$

where  $M$  is the x, y, or z component of the total center of mass,  $L$  is the x, y, or z component of the center of mass of a single object measured with respect to an arbitrary datum, and  $m_o$  is the mass of any particular object that has a unique density (this includes the shell, soft body, cameral gas, and cameral liquid for the models herein).

The center of buoyancy can be found by computing the center of mass of the water displaced by the baculite (i.e., center of volume). The stability of the model depends on the degree of separation between the centers of buoyancy and mass. Their true separation was found by using the theorem of Pythagoras on the x and z components of the models (ignoring the y components because of model symmetry). In order to apply to heteromorphic ammonoids, Okamoto (1996) redefines the stability index ( $S_t$ ) of Raup (1967):

$$S_t = \frac{\overline{BM}}{\sqrt[3]{V}} \tag{4}$$

where  $S_t$  is the stability index,  $\overline{BM}$  is the distance between the center of buoyancy and mass, and  $V$  is the entire volume occupied by the model ( $V_{wd}$  equal to defined above).

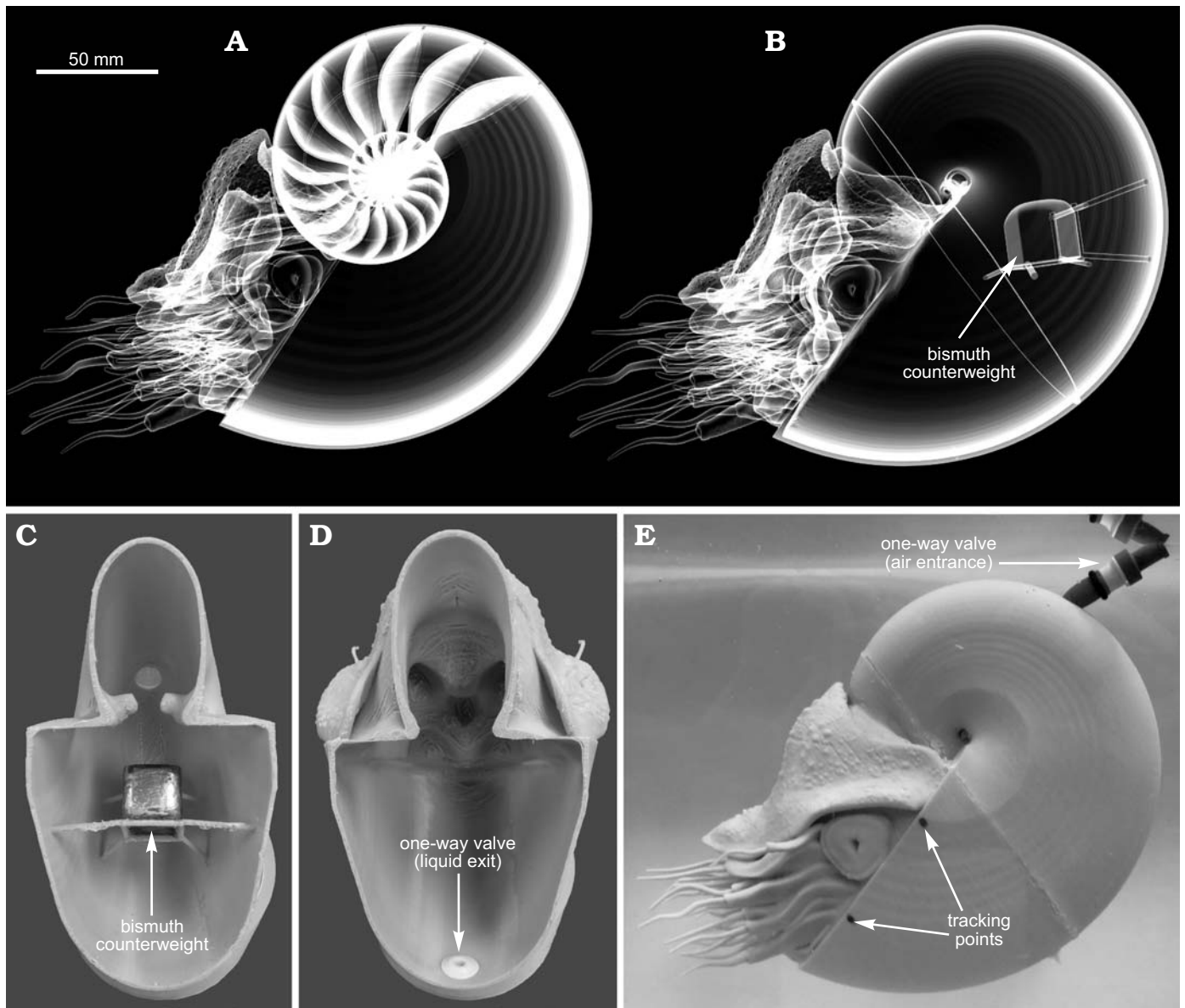


Fig. 4. Generation of a 3D printed model of *Nautilus pompilius* with theoretically equal physical properties to the virtual counterparts. **A.** Original virtual model from Peterman et al. (2019: fig. 2.5). **B.** Modified virtual model with simplified internal geometry. The center of buoyancy remains the same because external geometry does not change. The total center of mass, however, is corrected by a bismuth counterweight of known volume, density, and mass. **C.** 3D printed posterior half of the physical model with bismuth counterweight in the computed position. **D.** Anterior half of the physical model showing the one-way valve for liquid to exit upon displacement by an air-filled balloon. **E.** Neutrally buoyant physical model with the required volume to liquid ratio for neutral buoyancy. This computed volume of air is inserted through a one-way entrance valve into the internal balloon. Tracking points are placed parallel to the aperture in order to analyze movement in a hydrodynamic setting.

#### Restoring moment experiments with 3D printed models.—

Physical experimentation to investigate hydrostatics and hydrodynamics is hindered by the difficulty in creating models with the same mass (and distribution of that mass) as the living animal. This is primarily because morphometry and physical reconstruction are rather difficult in fossil shells (especially the ammonoids), and because there are no perfect model analogues for the materials of which the living animal was composed. In the current study, these caveats were addressed by modifying the virtual models (Fig. 4A) so that they had very simple internal geometry (Fig. 4B) while still having the same center of buoyancy as the origi-

nal virtual models. The differences in mass and total center of mass were corrected by 3D printing the modified virtual models in PLA filament, and then solving for the mass and position of a bismuth counterweight within the model (Fig. 4C, D). The position of the counterweight was solved by modifying Equation 3 as follows:

$$L_{Bi} = \frac{M \cdot \sum(m_o) - \sum(L \cdot m_o)}{m_{Bi}} \quad (5)$$

where  $L_{Bi}$  is the x, y, or z component of the counterweight and is the mass of the bismuth counterweight. This counterweight allows the models to be constructed with completely

different internal geometries and densities to the living animal (Fig. 4E), yet they still have theoretically equal hydrostatic properties (that is, the centers of mass and buoyancy). Since all physical experiments were performed in freshwater, the density of the water displaced ( $\rho_{wd}$ ) for these models was changed from  $1.025 \text{ g/cm}^3$  to  $1.000 \text{ g/cm}^3$ .

The densities of the PLA (after printing an object) and the bismuth counterweight were measured directly on reference objects that were constructed with simple geometries (2 cm cubes). The bismuth counterweights were casted by creating a positive model of the weight in Blender, surrounded by a base and walls in the horizontal directions. This positive model was then 3D printed and filled with high performance silicone rubber casting material. This process created a mold that could withstand the heat of melted bismuth ( $\sim 270^\circ\text{C}$ ) and with the required dimensions for each model. The 3D printed models required some ratio of gas and liquid so that they could achieve neutral buoyancy. After submerging the models and filling them with water, the computed volume of gas was inserted through a one-way valve into a latex balloon (Fig. 4E), which displaced the internal water through another one-way valve (Fig. 4D) until the desired ratio was achieved. This process was conducted for the *Nautilus pompilius* model and the *Baculites compressus* model. The 3D printed *B. compressus* model was scaled from a length of 86.4 cm to 60.0 cm in order to fit in the 1000 L tank where the restoration experiments were performed. The neutrally buoyant models of *N. pompilius* and *B. compressus* were rotated approximately  $38^\circ$  from their static syn vivo orientations and released. This angle was chosen because it was easy to measure for the *Nautilus* model and equals its syn vivo apertural angle measured from the vertical axis. The movement of each model was digitally recorded and analyzed with the physics modeling software, Tracker 4.11.0 (Brown 2017). Two points, parallel to the transverse plane, were placed on each of the models (Fig. 4E) and their X/Z coordinates were recorded as a function of time (Fig. 5). The angles of the apertures (where horizontally facing =  $0^\circ$ , downward vertical =  $-90^\circ$ , and upward vertical =  $+90^\circ$ ) were then computed from the relative positions of these tracking points.

*Experiments on active locomotion to overcome hydrostatic stability.*—The high hydrostatic stability of orthoconic cephalopods relative to other morphotypes was explored in terms of active locomotion to deviate from a stable orientation. A second 3D printed model of *Baculites compressus* was created following the same procedure as the first model. However, this model included an empty space for an axle located at the pivot point of rotation (i.e., the midpoint between the centers of buoyancy and mass). The axle was suspended by a ring stand clamp and fixed to two ball bearings to minimize friction while the baculite rotated. A 1-m long lightweight segment of silicone tubing with an inner diameter of 6.35 mm was fixed to the baculite perpendicular to the aperture (pointing in the ventral direction) to act as the source of thrust. Because little is known about the soft

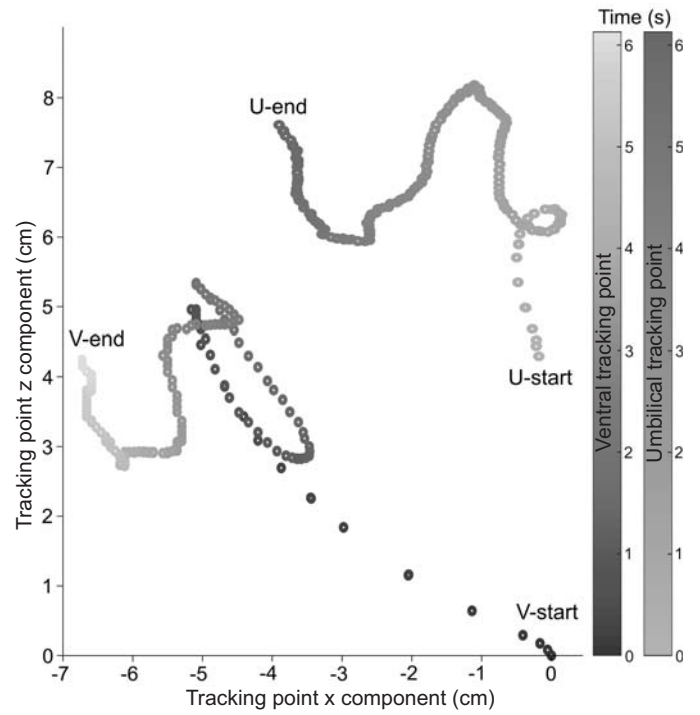


Fig. 5. Position of the ventral tracking point (V) and umbilical tracking point (U) as a function of time measured with the physics modeling software (Tracker 4.11.0; Brown 2017). Note that the rotation of the aperture is coupled with translational motion, resulting in complex movement.

body of the baculitids (and generally all ammonoids), the amount of thrust they could generate with their mantle cavity and hyponome is highly speculative. Therefore, we use thrust values that fall within the range of extant cephalopod analogues during experimentation (Table 1). Because thrust is dependent upon size (Chamberlain 1990; Thompson and Kier 2002), the thrust efficiency can be quantified by the thrust ratio (maximum propulsive thrust/total weight). This metric of efficiency is generally larger in coleoids, however,

Table 1. Thrust ratio (maximum propulsive thrust/total weight), thrust generated with the weight of the *Baculites compressus* model (thrust ratio  $\times 9.8 \text{ m/s}^2 \times 0.153 \text{ kg}$ ), funnel ratio (max cross-sectional area of funnel/volume<sup>2/3</sup>), and hyponome diameter for *Nautilus pompilius*, *Sepia officinalis*, and *Loligo vulgaris* reported in Chamberlain (1990). Three scenarios of possible thrusts generated to monitor rotation of a 3D printed model of *B. compressus* (experiment described below). Scenario 1: a continuous thrust applied to the 3D printed model with a ratio similar to *Nautilus*. Scenario 2: thrust from a simulated mantle cavity of 20% soft body volume of *B. compressus*. Scenario 3: a coleoid-like thrust ratio applied to the model.

|                           | Thrust ratio | Thrust            | Funnel ratio | Hyponome diameter (mm) |
|---------------------------|--------------|-------------------|--------------|------------------------|
| <i>Nautilus pompilius</i> | 0.2          | 0.30              | 0.035        | ?                      |
| <i>Sepia officinalis</i>  | 0.7          | 1.05              | 0.037        | ?                      |
| <i>Loligo vulgaris</i>    | 1.5          | 2.25              | 0.030        | ?                      |
| Scenario 1                | 0.169        | $0.254 \pm 0.020$ | 0.034        | 5.50                   |
| Scenario 2                | 0.255        | $0.384 \pm 0.021$ | 0.034        | 5.50                   |
| Scenario 3                | 1.069        | $1.607 \pm 0.144$ | 0.045        | 6.35                   |

*Nautilus* is actually more efficient in terms of its metabolic cost of locomotion (Neil and Askew 2018). The thrust ratio for several living cephalopods (see Chamberlain 1990) was multiplied by the weight of the baculite model to yield estimates of thrust that the baculite could produce at several different levels of thrust efficiency. We used three scenarios of thrust generation during experimentation (summarized in Table 1) that fall within the range of the thrust ratios of the extant cephalopods: *Nautilus pompilius*, *Sepia officinalis* (common cuttlefish), and *Loligo vulgaris* (European squid). The resultant thrusts were calibrated with a Vernier dual-range force sensor with a sensitivity of 0.01 N during 30 second intervals of recording at a sample interval of 30 samples per second.

Scenario 1 simulates a thrust at a similar efficiency to a *Nautilus pompilius* with an endless water supply (infinite mantle cavity volume). This was achieved by using a 10.7 liters per minute pump attached to the silicone tubing and reducing the exit cross-sectional area (reported as diameter in Table 1) until the desired thrust was approximated. Scenario 2 was performed by forcing a fixed volume of water through the tubing with a siphon pump. This fixed volume represents the total mantle cavity volume of the baculite model (estimated to be 20% of the soft body volume;  $0.20 \times 86.7 \text{ cm}^3 = 17.3 \text{ cm}^3$ ). Chamberlain (1990) stated that the effective mantle cavity volume in coleoids is about 70% of the total mantle cavity volume. Therefore, this value is a rather liberal estimate to test the difficulty in rotating from a stable vertical orientation. Scenario 3 was performed with a larger funnel ratio (Table 1) and larger mantle volume (the entire siphon pump volume of  $75 \text{ cm}^3$ ) to yield a high thrust ratio in between the values for *Sepia officinalis* and *Loligo vulgaris* (Table 1). Each of these thrust experiments provides a scenario to test how difficult it may have been for orthocones to deviate from their equilibrium position using active locomotion, by measuring the angle the baculite could rotate in response to thrust applied from the ventral direction.

## Results

**Virtual 3D models of *Baculites compressus*.**—The conditions for neutral buoyancy  $\Phi$ , hydrostatic stability ( $S_t$ ), and orientation are dependent upon the assumed densities for each model component. The hydrostatic influence of using different historical values for soft body and shell densities were computed and are organized in Table 2. High density values of  $1.068 \text{ g/cm}^3$  (Denton and Gilpin-Brown 1961) and  $2.94 \text{ g/cm}^3$  (Trueman 1941) for the soft body and shell, respectively, yield an 18.6% increase in  $\Phi$  (now emptying all camerae), and a 17.2% increase in stability index ( $S_t$ ). The very large value for shell density was assumed to have the same density as crystalline aragonite without any organic components. Lower density values of  $1.047 \text{ g/cm}^3$  (Hoffmann and Zachow 2011) and  $2.53 \text{ g/cm}^3$  (Collins et al. 1980) for the soft body and shell, respectively, yield a 9.3%

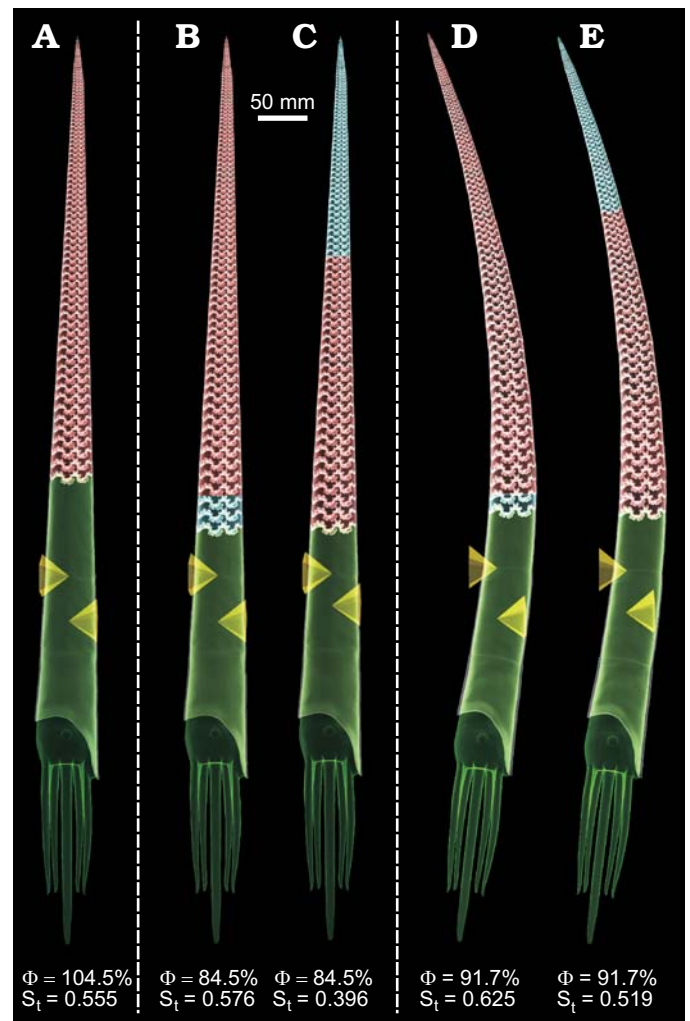


Fig. 6. Hydrostatic models of *Baculites compressus* with computed percentage of the phragmocone emptied for neutral buoyancy ( $\Phi$ ) and hydrostatic stability ( $S_t$ ). All models are oriented dorsum-left. The centers of buoyancy are marked by the tip of the higher pyramid. The total centers of mass are marked by the tip of the lower pyramid. Each material of unique density is designated a color (green, soft body; red, cameral gas; blue, cameral liquid; transparent grey, shell). **A.** Virtual model with 40% body chamber length to total length (BCL/L). **B.** Virtual model with 33% BCL/L and adorally distributed cameral liquid. **C.** Virtual model with 33% BCL/L and adapically distributed cameral liquid. **D, E.** *B. compressus* model modified with a concave dorsum similar to *B. grandis* and 33% BCL/L. Adorally (**D**) and adapically (**E**) distributed cameral liquid.

Table 2. Different density values applied to the *Baculites compressus* hydrostatic model with an even distribution of cameral liquid and gas. High and lower density ( $\rho$ ) values applied to the soft body (sb) and shell (sh) resulting in different percentages of the phragmocone to be emptied ( $\Phi$ ) and different stability indices ( $S_t$ ). Percent change in hydrostatic parameters is denoted by  $\% \Delta$ .

|                                     | $\rho_{sb}$<br>( $\text{g/cm}^3$ ) | $\rho_{sh}$<br>( $\text{g/cm}^3$ ) | $\Phi$<br>(%) | $S_t$ | $\% \Delta \Phi$ | $\% \Delta S_t$ |
|-------------------------------------|------------------------------------|------------------------------------|---------------|-------|------------------|-----------------|
| High $\rho$ ( $\text{g/cm}^3$ )     | 1.068                              | 2.94                               | 100.2         | 0.592 | 18.6             | 17.2            |
| Low $\rho$ ( $\text{g/cm}^3$ )      | 1.047                              | 2.53                               | 76.6          | 0.443 | -9.3             | -12.3           |
| Averaged $\rho$ ( $\text{g/cm}^3$ ) | 1.065                              | 2.62                               | 84.5          | 0.505 |                  |                 |

Table 3. The volumes ( $V$ , in  $\text{cm}^3$ ) and masses ( $m$ , in g) of the shell (sh), soft body (sb), cameral gas (cg), cameral liquid (cl), bismuth counterweight (Bi), total camerae (ct), water displaced (wd), and total mass for each virtual model. These metrics were used to compute the percentage of the phragmocone emptied for a neutrally buoyant condition ( $\Phi$ ). NA, not available.

| Virtual model  | $V_{\text{sh}}$ | $m_{\text{sh}}$ | $V_{\text{sb}}$ | $m_{\text{sb}}$ | $V_{\text{cg}}$ | $m_{\text{cg}}$ | $V_{\text{cl}}$ | $m_{\text{cl}}$ | $V_{\text{Bi}}$ | $m_{\text{Bi}}$ | $V_{\text{ct}}$ | $V_{\text{wd}}$ | $m_{\text{wd}}$ | $m_{\text{total}}$ | $\Phi$ |
|--|-----------------|-----------------|-----------------|-----------------|-----------------|-----------------|-----------------|-----------------|-----------------|-----------------|-----------------|-----------------|-----------------|--------------------|--------|
| <i>Nautilus pompilius</i>                              | 53.802          | 140.961         | 695.690         | 740.910         | 109.053         | 0.131           | 21.471          | 22.008          | NA              | NA              | 132.735         | 882.227         | 904.283         | 904.010            | 83.6   |
| <i>Nautilus pompilius</i> (modified)                   | 192.135         | 214.039         | NA              | NA              | 93.601          | 0.115           | 587.666         | 587.666         | 8.250           | 79.332          | 587.666         | 882.227         | 882.227         | 881.151            | 13.7   |
| <i>Baculites compressus</i> (40% BCL, emptied)         | 57.269          | 150.045         | 293.384         | 312.454         | 96.954          | 0.117           | 0.000           | 0.000           | NA              | NA              | 96.954          | 446.969         | 458.143         | 462.615            | 104.5  |
| <i>Baculites compressus</i> (33% BCL, adoral liquid)   | 61.771          | 161.840         | 259.099         | 275.941         | 107.218         | 0.129           | 19.729          | 20.222          | NA              | NA              | 126.946         | 446.969         | 458.143         | 458.120            | 84.5   |
| <i>Baculites compressus</i> (33% BCL, adapical liquid) | 61.771          | 161.840         | 259.099         | 275.941         | 107.218         | 0.129           | 19.729          | 20.222          | NA              | NA              | 126.946         | 446.969         | 458.143         | 458.132            | 84.5   |
| <i>Baculites compressus</i> (curved, adoral liquid)    | 66.124          | 173.246         | 250.033         | 266.285         | 113.511         | 0.137           | 10.239          | 10.495          | NA              | NA              | 123.750         | 439.174         | 450.153         | 450.162            | 91.7   |
| <i>Baculites compressus</i> (curved, adapical liquid)  | 66.124          | 173.246         | 250.033         | 266.285         | 113.140         | 0.136           | 10.610          | 10.875          | NA              | NA              | 123.750         | 439.174         | 450.153         | 450.162            | 91.7   |
| <i>Baculites compressus</i> (33% BCL, even gas)        | 20.661          | 54.132          | 86.664          | 92.297          | 35.859          | 0.043           | 6.603           | 6.768           | NA              | NA              | 42.461          | 149.503         | 153.241         | 153.241            | 84.5   |
| <i>Baculites compressus</i> (33% BCL, Modified 1)      | 76.244          | 84.936          | NA              | NA              | 54.989          | 0.067           | 12.913          | 12.913          | 5.357           | 51.496          | 67.902          | 149.503         | 149.503         | 149.412            | 80.8   |
| <i>Baculites compressus</i> (33% BCL, Modified 2)      | 76.381          | 85.089          | NA              | NA              | 72.332          | 0.089           | 0.000           | 0.000           | 6.674           | 64.150          | 72.332          | 149.503         | 149.503         | 149.327            | 100    |

decrease in  $\Phi$  and a 12.3% decrease in  $S_t$ . The *Baculites compressus* model is very stable in a vertical orientation for each of these simulations with both high and low density values (Table 2).

The averaged bulk density of  $1.065 \text{ g/cm}^3$  was adopted from Westermann (2013) because of the unknown volumes of the dense, calcified aptychi and the low-density mantle cavity filled with seawater. However, this value was roughly tested by assuming a mantle cavity of 15–20% soft body volume, and aptychi of similar proportions to *Baculites* sp. reported in Kruta et al. (2009). The average length aptychi of 27 mm were scaled to fit the 58 mm aperture of the current *Baculites compressus* model. Kruta et al. (2009) reported aptychi thicknesses between 600  $\mu\text{m}$  and 1 mm depending on the rugae. Linearly scaling the averaged thickness of 800  $\mu\text{m}$  to the length of the aperture yielded aptychi that were 1.75 mm thick with a mass of 6.22 g (assuming an aptychi density of  $2.71 \text{ g/cm}^3$ ). The bulk density computed from the mass of the soft body with a density of the *Nautilus* ( $1.06 \text{ g/cm}^3$ ; Hoffmann et al. 2015), and the masses of the mantle cavity and aptychi was  $1.066 \text{ g/cm}^3$  (a 0.1% difference from the value used herein and in Westermann 2013). A 15% mantle cavity would yield a bulk density of  $1.069 \text{ g/cm}^3$  (approximately a 0.4% difference). These differences would not considerably influence the total mass distribution of the organism (but compare other morphotypes with larger aptychi; Parent et al. 2014).

The masses and volumes of each virtual model component are listed in Table 3, and their spatial distributions are listed in Table 4. Comparison of the total mass ( $m_{\text{total}}$ ) and mass of the water displaced ( $m_{\text{wd}}$ ) yields the error in

buoyancy calculations which should theoretically be equal for neutrally buoyant objects. Each of the neutrally buoyant, virtual models in this study have less than 1% difference between these two metrics. This source of error is most likely due to subtle volume changes in the digital mesh induced by trying to manage the .stl file sizes.

Two 3D baculite models of differing body chamber lengths to total length ratios (40 and 33% BCL/L) were reconstructed with measured shell and septum thicknesses (Fig. 2). These values fall within the upper and lower estimates of the “mesodome” category termed by Westermann (2013). The larger body chamber model (Fig. 6A) requires a cameral gas volume that is 104.5% of the available volume of the phragmocone to be neutrally buoyant. This 40% BCL/L model (Fig. 6A) is completely emptied (filled with 100% cameral gas) in order to compute its hydrostatic stability ( $S_t = 0.555$ ) with a slightly negative buoyancy. The 33% BCL/L models require 84.5% of their cameral volumes to be emptied of cameral liquid in order to be neutrally buoyant. Distributing the volume of cameral liquid required for neutral buoyancy in the adoral direction (Fig. 6B) and the adapical direction (Fig. 6C) influences the hydrostatic stability of each of these models (0.576 and 0.396, respectively). However, these values are still rather high and orientation is unchanged from vertical.

The mass distribution and hydrostatic properties for baculitids with a concave dorsum were investigated by modifying the 33% BCL/L *B. compressus* model (Fig. 6D, E). A shell with a concave dorsum similar to the younger (early Maastrichtian) species *Baculites grandis* requires slightly less cameral liquid to be neutrally buoyant. The apertural

Table 4. The center of buoyancy and centers of mass for each model component (x, z, in mm) in the virtual models. These values, along with the metrics in Table 3 were used to compute hydrostatic stability ( $S_t$ ). The y component is ignored because all models are bilaterally symmetric. BCL, body chamber ratio;  $\overline{BG}$ , distance between centers of buoyancy and gravity; Bi, bismuth; NA, not available.

| Virtual model  | Center of buoyancy |         | Center of mass (soft body) |         | Center of mass (shell or plastic) |         | Center of mass (cameral liquid) |         | Center of mass (cameral gas) |        | Center of mass (Bi weight) |         | Center of mass (total) |         | $\overline{BG}$ (mm) | $S_t$ |
|--|--------------------|---------|----------------------------|---------|-----------------------------------|---------|---------------------------------|---------|------------------------------|--------|----------------------------|---------|------------------------|---------|----------------------|-------|
|  | x                  | z       | x                          | z       | x                                 | z       | x                               | z       | x                            | z      | x                          | z       | x                      | z       |                      |       |
| <i>Nautilus pompilius</i>                              | -30.715            | -13.577 | -22.402                    | -18.522 | -46.349                           | -15.664 | -71.196                         | 9.993   | -69.245                      | 13.937 | NA                         | NA      | -27.331                | -17.378 | 5.090                | 0.053 |
| <i>Nautilus pompilius</i> (modified)                   | -30.715            | -13.577 | NA                         | NA      | -11.380                           | 9.818   | -28.784                         | -24.928 | -84.834                      | 15.303 | -59.514                    | -34.867 | -27.331                | -17.378 | 5.090                | 0.053 |
| <i>Baculites compressus</i> (40% BCL, emptied)         | -139.751           | 2.093   | -61.237                    | 3.567   | -172.157                          | 0.406   | NA                              | NA      | -359.497                     | -1.407 | NA                         | NA      | -97.257                | 2.515   | 42.466               | 0.555 |
| <i>Baculites compressus</i> (33% BCL, adoral liquid)   | -139.751           | 2.093   | -42.004                    | 3.858   | -174.241                          | 0.442   | -198.763                        | 1.518   | -346.517                     | -1.156 | NA                         | NA      | -95.721                | 2.547   | 44.033               | 0.576 |
| <i>Baculites compressus</i> (33% BCL, adapical liquid) | -139.751           | 2.093   | -42.004                    | 3.858   | -174.241                          | 0.442   | -510.032                        | -4.386  | -289.257                     | -0.070 | NA                         | NA      | -109.447               | 2.286   | 30.305               | 0.396 |
| <i>Baculites compressus</i> (curved, adoral liquid)    | -67.873            | 43.649  | 29.614                     | 47.354  | -90.362                           | 38.966  | -128.910                        | 29.912  | -264.809                     | 39.369 | NA                         | NA      | -20.344                | 43.717  | 47.529               | 0.625 |
| <i>Baculites compressus</i> (curved, adapical liquid)  | -67.873            | 43.649  | 29.614                     | 47.354  | -90.362                           | 38.966  | -460.137                        | 72.862  | -234.193                     | 35.372 | NA                         | NA      | -28.421                | 44.740  | 39.451               | 0.519 |
| <i>Baculites compressus</i> (33% BCL, even gas)        | -112.702           | 0.665   | -44.807                    | 1.901   | -136.618                          | -0.470  | -240.275                        | -1.291  | -240.275                     | -1.291 | NA                         | NA      | -85.927                | 0.922   | 26.776               | 0.505 |
| <i>Baculites compressus</i> (33% BCL, Modified 1)      | -112.702           | 0.665   | NA                         | NA      | -142.672                          | 0.111   | -4.419                          | 2.238   | -106.395                     | 1.004  | -12.748                    | 1.929   | -85.927                | 0.922   | 26.776               | 0.505 |
| <i>Baculites compressus</i> (33% BCL, Modified 2)      | -112.702           | 0.665   | NA                         | NA      | -142.593                          | 0.109   | NA                              | NA      | -81.291                      | 1.248  | -10.773                    | 2.000   | -85.927                | 0.922   | 26.776               | 0.505 |

Table 5. Mass (in g) discrepancies between the modified virtual models with simple internal geometries and their 3D printed counterparts for each model component. The error in hydrostatic stabilities ( $S_t$ ) were computed by assuming that the mass surplus or deficit was acting in the positive and negative z-directions only (representing maximum error in  $S_t$ ).  $\Phi$ , neutrally buoyant condition; NA, not available.

| Object               | <i>Nautilus pompilius</i> (modified) |             | <i>Baculites compressus</i> (Modified 1) |             | <i>Baculites compressus</i> (Modified 2) |             |
|----------------------|--------------------------------------|-------------|--|-------------|--|-------------|
|                      | virtual mass                         | actual mass | virtual mass                             | actual mass | virtual mass                             | actual mass |
| PLA shell            | 214.040                              | 194.900     | 84.936                                   | 85.450      | 85.089                                   | 79.306      |
| Bismuth weight       | 79.332                               | 79.332      | 51.496                                   | 51.496      | 64.150                                   | 64.150      |
| Air valve            | NA                                   | 2.113       | NA                                       | 2.113       | NA                                       | 2.113       |
| Balloon              | NA                                   | 0.224       | NA                                       | 0.224       | NA                                       | 0.224       |
| Glue                 | NA                                   | 1.171       | NA                                       | 2.154       | NA                                       | 1.900       |
| Total (empty)        | 293.372                              | 277.740     | 136.590                                  | 141.437     | 149.503                                  | 147.693     |
| Mass discrepancy (%) | -5.340                               |             | 3.427                                    |             | -1.210                                   |             |
| $S_t$                | 0.053                                |             | 0.505                                    |             | 0.505                                    |             |
| $S_t$ Error          | 0.002                                |             | 0.035                                    |             | 0.013                                    |             |
| Virtual $\Phi$       | 13.7                                 |             | 80.8                                     |             | 100.0                                    |             |
| Actual $\Phi$        | 11.4                                 |             | 85.0                                     |             | 97.3                                     |             |

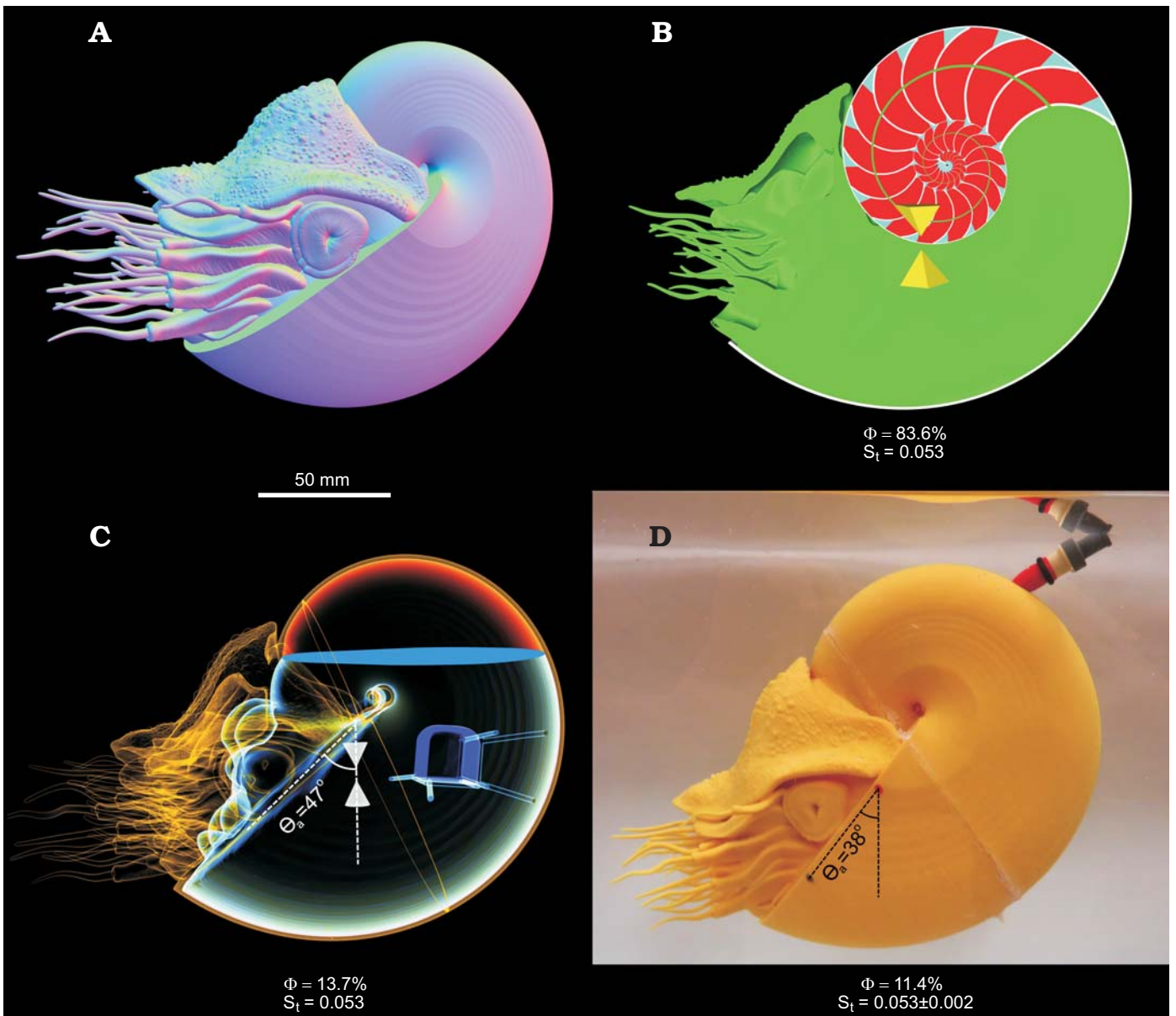


Fig. 7. Virtual and physical hydrostatic models of *Nautilus pompilius* with computed percentage of the phragmocone emptied for neutral buoyancy ( $\Phi$ ) and hydrostatic stability ( $S_t$ ). The tip of the up-side-down pyramid = center of buoyancy. The tip of the right-side-up pyramid = total center of mass. **A.** External view of the virtual model. **B.** Medial section of the virtual model with each component of unique density (green, soft body; red, cameral gas; blue, cameral liquid; grey, shell). **C.** Modified virtual model with simplified internal geometry and bismuth counterweight (yellow, PLA plastic; red, air; blue, liquid; purple, bismuth counterweight). **D.** Neutrally-buoyant, 3D printed model. The differences in  $\Phi$  and the apertural angle ( $\theta_a$ ) are a result of the mass discrepancy (Table 5) and irregular geometry of the balloon. The error in  $S_t$  was computed assuming that the total mass discrepancy was distributed in the positive or negative z-directions.

angle at rest is rotated from about  $5^\circ$  from the vertical axis in the dorsal direction when compared to the straight, vertical models.

**Restoring moment of *Nautilus pompilius*.**—The virtual *Nautilus pompilius* model (Fig. 7A, B) is neutrally buoyant when 83.6% of its cameral volume is emptied. The hydrostatic stability of this model ( $S_t = 0.053$ ) is about an order of magnitude lower than the virtual baculite models (Fig. 6). The modified virtual *N. pompilius* model (Fig. 7C) requires less cameral gas to be neutrally buoyant because

it has a larger cavity volume due to the added mass of the bismuth counterweight (Table 3). The neutrally buoyant, 3D printed *N. pompilius* model (Fig. 7D) has a very similar mass distribution to the virtual models, but is slightly different due to discrepancies in the total masses between the two. Removing support material after 3D printing, and drilling holes in the plastic for the one way valves have resulted in a slightly lower mass in the physical model than the virtual model. This translates to a negative mass discrepancy of 5.340% (Table 5). This lower mass requires less gas in the cavity to be neutrally buoyant (11.4%) and can cause the

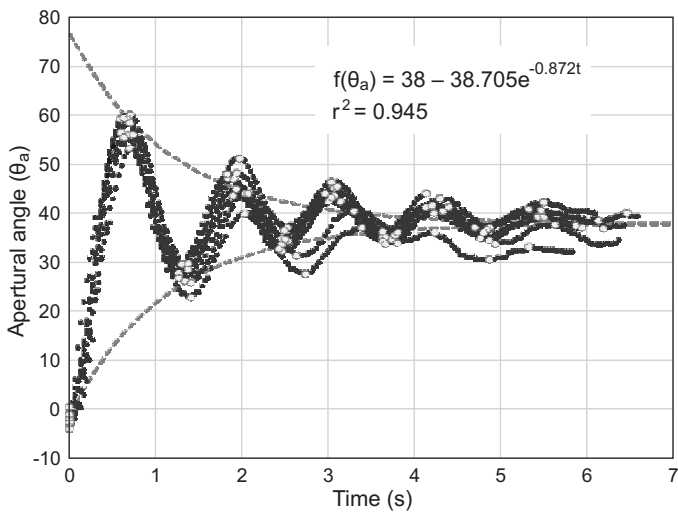


Fig. 8. Hydrodynamic restoration of the *Nautilus pompilius* 3D printed model following underdamped harmonic oscillation. Apertural angle ( $\theta_a$ ) measured in degrees as a function of time after rotating approximately  $38^\circ$  from the equilibrium orientation. An angle of zero represents a condition where the aperture is horizontally oriented. Open dots represent the peaks used to calculate decay in amplitude with time (grey dashed curves).

stability index to vary by 0.002. The variability in the stability index is computed by shifting the deficient mass in the positive and negative  $z$  directions. The balloon also becomes convex as it displaces the liquid in the cavity, which contrasts with the flat interface of the virtual model. This difference also subtly influences the mass distribution and is responsible for the differing orientations of the aperture between the virtual and physical models (Fig. 7C, D).

The restoring moment of the 3D printed *Nautilus* model was periodic and caused the aperture to oscillate back and forth (Fig. 8) about the equilibrium orientation ( $\theta_a$  of  $38^\circ$ ). This motion is characterized as underdamped harmonic oscillation because each progression decreases in amplitude and increases in wavelength as a function of time. Each of the 10 trials resulted in very similar paths that took approximately 7 seconds to stabilize.

**Restoring moment of *Baculites compressus*.**—After scaling the original virtual model of *Baculites compressus* to 60.0 cm, it was altered to have a somewhat even distribution of cameral liquid and gas in each camera. This distribution was approximated by setting the individual centers of mass for the cameral liquid and cameral gas equal to the center of volume of all of the camerae (Fig. 9A). This condition resulted in a stability index (0.505) in between the adorally and adapically distributed cameral liquid scenarios (Fig. 6B, C). The virtual *B. compressus* model modified to have a simple internal geometry (Fig. 9B) required 80.8% of its cavity to be filled with liquid in order to be neutrally buoyant. After 3D printing this model (Fig. 9C), residual support material and glue resulted in a positive mass discrepancy of 3.427% (Table 5). This increase in mass requires to be increased to 85.0% and translates to a maximum error in  $S_i$  of 0.035.

The 3D printed model of *Baculites compressus* (Fig. 9C) is fundamentally different from the *Nautilus pompilius* model during hydrodynamic restoration from the same angle of displacement ( $38^\circ$ ). Instead of oscillating around the equilibrium position, the baculite model experiences a quick decay to its stable, vertical orientation (Fig. 10). This type of motion is characterized as overdamped harmonic motion. The seven trials of the *B. compressus* hydrodynamic restoration (Fig. 10) were more chaotic than the *N. pompilius* experiment (Fig. 8), but the original restoring orientation was reached in approximately half the time (just over 3 seconds). It should be noted that there was a significant amount of translation in addition to the rotational movement during hydrodynamic restoration. This was likely due to the differences in drag between the portions of the shell above and below the pivot point (which have different cross sectional areas and probably drag coefficients that both positively influence the force of drag).

**Thrust required to overcome the *Baculites compressus* restoring moment.**—The *B. compressus* model used to test thrust (Modified 2 in Tables 3 and 4, Fig. 9E) had a negative mass discrepancy of 1.210%, which corresponds to a maximum error in stability index of 0.013. This mass discrepancy also influenced the required cameral liquid for neutral buoyancy, but  $\Phi$  was held at 100% for this experiment because there was no way to verify neutral buoyancy from this stationary model.

Thrust was applied to the venter of the model during three scenarios to generate rotation (see Table 1): (i) a continuous thrust near the value computed from the thrust ratio of *Nautilus pompilius* (Fig. 11A), (ii) periodic pulses from the computed mantle cavity volume ( $17.3 \text{ cm}^3$ ) and realistic funnel ratio (0.034; Table 1) of the scaled *Baculites compressus* virtual model (Fig. 11B), and (iii) larger periodic thrusts between the thrust ratios for *Sepia officinalis* and *Loligo vulgaris* (Fig. 11C). During scenario 1, the thrust produced ( $0.254 \pm 0.020 \text{ N}$ ) resulted in an average displacement from the vertical resting orientation of  $22.7^\circ$  in the dorsal direction. This thrust value is similar to the value computed from the relatively low thrust ratio of the extant *N. pompilius* (Table 1) and follows the conditions of an infinite mantle cavity (constant thrust). Scenario 2 operates under the condition of a finite mantle cavity volume ( $17.3 \text{ cm}^3$ ) that produces  $0.384 \pm 0.021 \text{ N}$  of thrust. This value of thrust corresponds to a slightly larger thrust ratio than *N. pompilius* (Table 1) and results in an average peak rotation of  $25.6^\circ$ . In order to produce larger values of thrust (in between the thrust ratios of the coleoids *Sepia officinalis* and *Loligo vulgaris*;  $1.607 \pm 0.144 \text{ N}$ ), a volume of  $75 \text{ cm}^3$  was expelled through a larger jet orifice, resulting in an average peak rotation of  $72.2^\circ$  from the resting vertical position.

It may be important to consider several sources of error during physical experimentation. The bearings were chosen to reduce the friction of rotation along the axle; however, some value of friction must still be present. The silicone

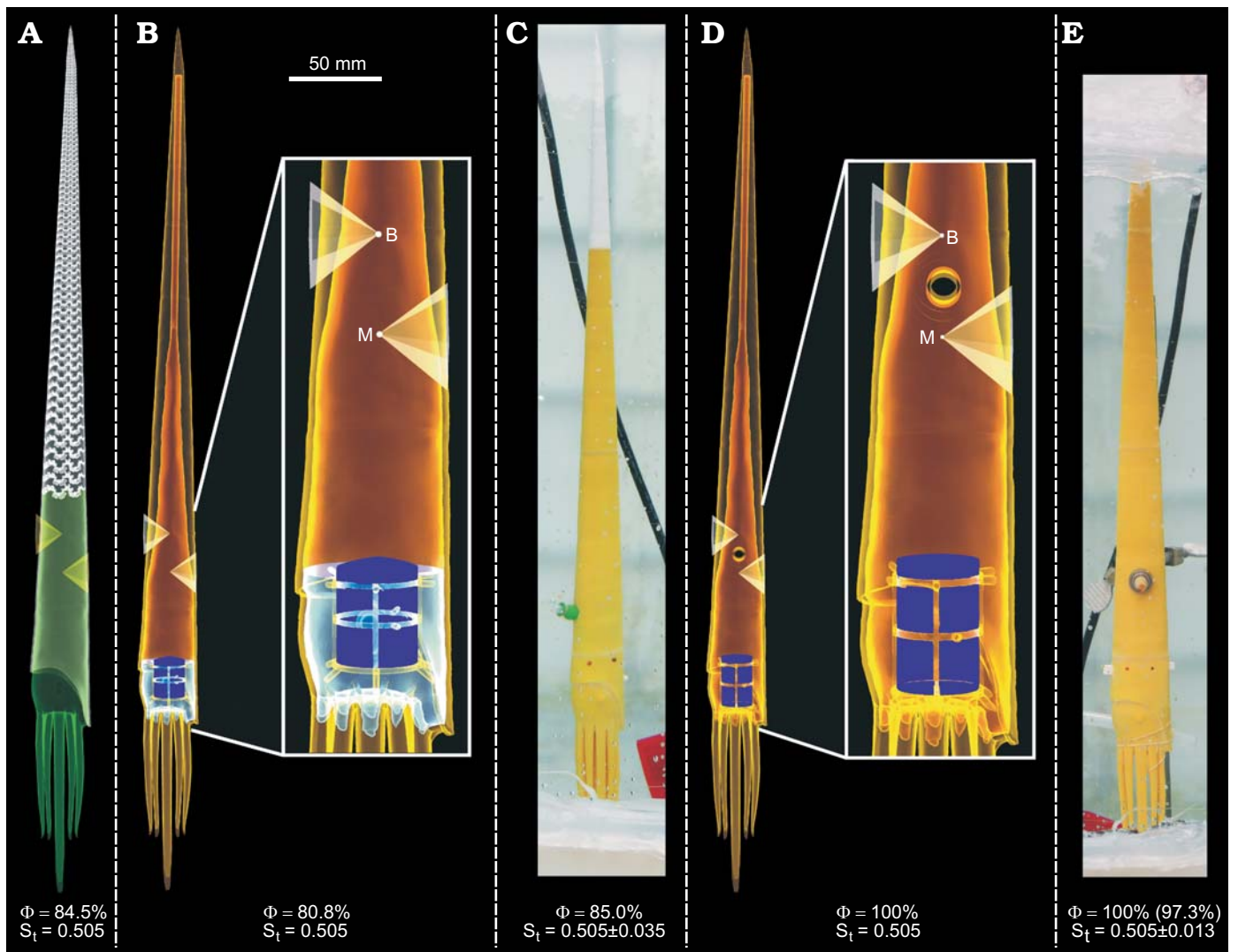


Fig. 9. Virtual and physical hydrostatic models of *Baculites compressus* with computed percentage of the phragmocone emptied for neutral buoyancy ( $\Phi$ ) and hydrostatic stability ( $S_t$ ). Green, soft body; grey, shell; red, gas; blue, liquid; yellow, PLA plastic; purple, bismuth counterweight; B, center of buoyancy; M, center of mass. **A.** Virtual model with an even distribution of cameral liquid and gas in the phragmocone (center of mass of cameral liquid and gas = center of volume of the phragmocone; cameral liquid and gas not shown). **B.** Modified virtual model with simplified internal geometry (“Modified 1” in Table 3). **C.** Neutrally-buoyant, 3D printed model. **D.** Modified virtual model with simplified internal geometry and axel hole through pivot point of rotation (“Modified 2” in Table 3). **E.** Neutrally-buoyant, 3D printed model fixed to an axel and silicone tubing used to supply thrust in the ventral direction. For this model, the mass discrepancy (Table 5) resulted in a slightly lower of 97.3%, but was held constant at 100%. All computed errors in  $S_t$  were computed assuming that the total mass discrepancy was distributed in the positive or negative z-directions.

tubing that supplied thrust at the venter of the shell also had some weight and drag. Each of these factors could have made it more difficult for the baculite to move through the water.

## Discussion

**Hydrostatic properties of *Baculites compressus*.**—All of the *Baculites compressus* models in the current study have the capacity to be neutrally buoyant (or nearly so). Body chamber length is a limiting factor on neutral buoyancy because larger soft bodies contribute more towards the total organismal mass and result in fewer camerae that can be emptied to regulate the weight of the living cephalopod. As

the body chamber ratio decreases for a neutrally buoyant orthocone, it would become positively buoyant unless some volume of cameral liquid filled the phragmocone. Modifying the body chamber ratio in *B. compressus* (Fig. 6A vs. 6B, C) shows that syn vivo orientation and hydrostatic stability ( $S_t$ ) do not change very much between the upper and lower limits of the mesodome category (40% and 33%; Westermann 2013). The largest difference in hydrostatic properties between these two models is the ratio of cameral liquid and gas in the phragmocone for a neutrally buoyant condition ( $\Phi$ ). The model with the larger body chamber ratio is only slightly negatively buoyant, with an effective mass of 4.4 g. A very slight negative buoyancy is easier to manage by the living cephalopod and is commonly observed in the extant

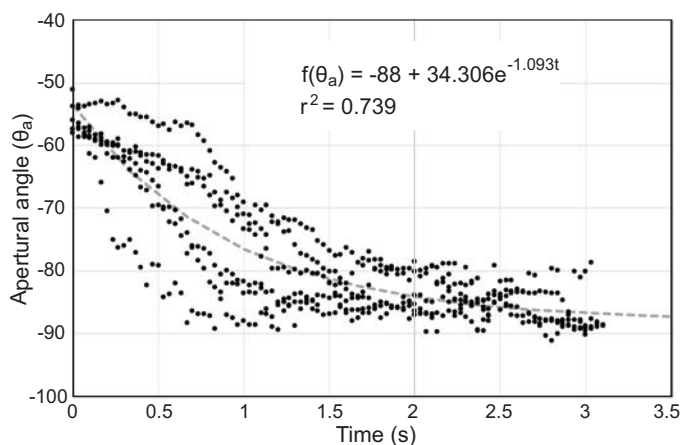


Fig. 10. Hydrodynamic restoration of the *Baculites compressus* 3D printed model following overdamped harmonic motion. Apertural angle ( $\theta_a$ ) measured in degrees as a function of time after rotating approximately  $38^\circ$  from the equilibrium orientation. An angle of  $-90^\circ$  represents a condition where the aperture is directed downwards. The function of decay in  $\theta_a$  with time is represented by the grey dashed curve. Note that this model restores more quickly and does not oscillate about the equilibrium orientation.

*Nautilus* (Ward 1987). This can also be accomplished with more cameral liquid than what is required for perfect neutral buoyancy. However, as the body chamber ratio increases, this effective mass will become too large to be considered negligible.

The virtual baculite models (Fig. 6) all assume a stable vertical orientation, even when distributing the cameral liquid within the phragmocone in the adapical direction (Fig. 6C). The hydrostatic stability of *Baculites compressus* is around an order of magnitude higher than the *Nautilus pompilius* ( $S_t = 0.05$ ; see Peterman et al. 2019: fig. 2.6). Changing the distribution of cameral liquid would not allow the baculite to deviate from a vertical static orientation. Adapically distributed cameral liquid only slightly reduces stability and does not cause the shell to rotate to a dorsum upward orientation. This horizontal orientation would require mass displacement in the ventral direction (to situate the center of mass under the center of buoyancy), which is not practical for the orthoconic morphotype. One feasible way to modify the orientation of these orthoconic models in a neutrally buoyant, static setting is to reduce stability until the centers of buoyancy and mass coincide. Under this scenario, there is no preferred orientation and active locomotion could be used to modify orientation. This has been experimentally demonstrated by Westermann (1977, 2013) by using 2D “*Orthoceras*” models and postulated by Klinger (1980), Westermann (1996), and Tsujita and Westermann (1998). However, the virtual *B. compressus* models in the current study (Fig. 6C) would require much more cameral liquid to reduce hydrostatic stability. As the phragmocone becomes completely filled, stability would approach a value near zero, and buoyancy would decrease significantly (Peterman and Barton 2017). Adapically distributing cameral liquid is much less effective than higher density

counterweights such as cameral deposits or endosiphuncular deposits employed by Paleozoic orthocones (Teichert 1964; Mironenko 2018; Peterman et al. 2019). There is also no evidence that suggests siphunculate cephalopods had the ability to selectively choose which chambers are flooded or emptied (Ward 1979). Also, some portion of cameral liquid would be retained by capillary retention within complex septal recesses (Peterman and Barton 2019) which would partially distribute the center of mass of the cameral liquid toward the center of the phragmocone, rather than adapically or adorally. Therefore, an even distribution of cameral liquid and gas in the phragmocone is more realistic; that is, after the camera behind a newly formed septum is sufficiently emptied.

Westermann (1996, 2013) has suggested that large orthocones with a concave dorsum (such as *B. grandis*) were able to rest horizontally in the water column by situating their center of mass in the ventral direction under the center of buoyancy. As discussed above, the required cameral liquid to move the center of mass close to the center of buoyancy would cause the model to become negatively buoyant. Additionally, a ventrally displaced total center of mass can only be achieved by distributing more mass in the ventral direction (or an absence of mass in the dorsal direction). The *B. compressus* models modified with a concave dorsum similar to *B. grandis* (Fig. 6D, E) show that a horizontal orientation is not likely to occur in a static setting. These models have high stability indices even when the cameral liquid is distributed adapically (Fig. 6E). The only significant change is that the aperture is rotated about  $5^\circ$  from the vertical axis in the dorsal direction. This could have improved the field of view in the dorsal direction, which could have been useful in the water column or in a demersal setting. The difference in size between the virtual models and larger orthocones is relative ( $S_t$  is independent of size) and would only matter in a hydrodynamic setting (from differences in Reynolds numbers).

**Restoring moments of the stable, orthoconic morphotype.**—Since the restoring moment is essentially a torque, it is proportionate to the distance between the centers of mass and buoyancy. Therefore, neutrally buoyant objects with a higher hydrostatic stability ( $S_t$ ) have a greater restoring moment acting upon them after they are displaced from their static equilibrium position. These properties are fundamentally different between the *Nautilus pompilius* model (Fig. 7D) and the *Baculites compressus* model (Fig. 9C) because the latter has a hydrostatic stability value that is approximately an order of magnitude larger than the former. Hydrodynamic restoration is also dependent upon the force of drag, that is proportionate to the cross-sectional area of the object moving through the liquid and its drag coefficient (a metric inversely proportionate to the degree of streamlining). Underdamped harmonic oscillation, observed in the *N. pompilius* restoration experiment (Fig. 8), is diagnostic for neutrally buoyant objects with low hydrostatic stability rel-

ative to the force of drag during restoration. In contrast, the *B. compressus* model has high hydrostatic stability that exerts a larger restoring moment after it is displaced. This rotational movement also experiences much more drag, which prevents oscillation around the vertical equilibrium orientation. These hydrodynamic properties during restoration result in overdamped harmonic motion, causing the *B. compressus* model to reach its resting orientation in about half the time as the *N. pompilius* model (compare Figs. 8 and 10).

**Were orthoconic cephalopods able to overcome their restoring moments?**—As demonstrated by the virtual *Baculites compressus* models (Fig. 6) and the hydrodynamic restoration experiment (Fig. 10), this species (and generally the orthoconic morphotype) is very stable in a vertical orientation and would rely upon active locomotion in order to significantly alter their position. The thrust efficiency of baculitids is unknown and may be independent of retractor muscle size. Jacobs and Landman (1993) propose a coleoid-like swimming mechanism for ammonoids that differ from the *Nautilus* by contracting the mantle cavity rather than retracting the head complex into the body. However, the constraints of being enclosed within a rigid shell and the ammonoid mechanism for propulsion (effective musculature) are largely unknown. Therefore, the true baculitid thrust ratio is probably not significantly lower than the *N. pompilius* ratio, and probably does not exceed the values of the very efficient, shell-less coleoids.

The magnitude of thrust generated by compressing the mantle cavity is dependent upon the mantle cavity volume, cross sectional area of the jet orifice, and the time over which the mantle liquid is expelled. A constant thrust (simulating an infinite mantle cavity volume) with a thrust ratio near that of the *Nautilus pompilius* does not significantly allow the baculite to alter its orientation (Fig. 11A). This scenario is unrealistic in the sense that a jet pulse is followed by a period of refilling. During this time, the restoring moment acting on the baculite will begin to return it to its vertical equilibrium position (where  $\theta_a = -90^\circ$ ). A finite mantle cavity pulse generated from the computed *B. compressus* mantle cavity ( $17.3 \text{ cm}^3$ ) is a more realistic scenario. However, the thrust produced is only slightly larger than the thrust computed from the *N. pompilius* thrust ratio. This similarly does not allow the baculite to significantly alter its orientation (Fig. 11B). Larger angles of offset ( $\theta_a$ ) yield larger restoring moments and require sufficient thrusts applied at the aperture to overcome them. A much larger average peak force that corresponds to a thrust ratio in between *Sepia officinalis* and *Loligo vulgaris* is generated by using a larger mantle cavity volume. This volume produces a thrust relative to the weight of *B. compressus* within the coleoid range, but would require the expulsion of a mantle cavity that is 86% of the volume of the entire body chamber. Perhaps these values of thrust could be obtained from the appropriate mantle cavity volume if it was expelled at lower time intervals. However, shortening the pumping intervals in this

study caused pump failure, which questions the ability of the living baculite to withstand such pressures in the mantle cavity. If the practicality of generating such thrusts is ignored, it is still unlikely that the living cephalopods would have expended such a large amount of energy. The thrust ratios reported by Chamberlain (1990) and used herein are a measurement of the maximum propulsive burst normalized by the organismal weight. The maximum propulsive burst (as observed in escape jetting) is much different from normal locomotion because the resting mantle cavity volume is increased by hyperinflation (Anderson and Demont 2000); an ability that may have been hindered by being enclosed within a rigid shell. The degrees of rotation induced by the liberal values of thrust used in this study suggest that a horizontal or sub-horizontal form of locomotion is very unlikely in baculitids and other orthoconic cephalopods with similar stability indices (i.e., Paleozoic orthocones without cameral or endosiphuncular deposits; Peterman et al. 2019).

**Insights on the mode of life for highly-stable orthoconic cephalopods.**—

The highly-stable, vertical syn vivo orientation of *Baculites compressus* and other orthocones with similar shell geometries makes it difficult to deviate from this equilibrium position. Traditional methods of active locomotion (jet propulsion) may not have generated enough thrust to overcome the restoring moment acting on the shell at higher angles of offset. The unknown soft body morphology of the baculitids is problematic when interpreting their mode of life and habit. The models in the current study had rigid arms that did not move. During life, a baculitid may have been able to use these arms to aid in locomotion, especially if a webbing connected each of the arms. In this case, the living baculite could have modified its drag by spreading its tentacles to help prevent falling to a vertical position. The position of the arms could also generate lift during movement through the water. However, both of these scenarios remain entirely speculative because there is no unequivocal preservation of ammonoid arms (Klug and Lehmann 2015).

It probably would have been rather cumbersome for the hyponome to bend around the ventral rostrum present on many baculitid shells (as noted by Westermann 2013). This long ventral rostrum, along with lateral sinuses, led Westermann (2013) to revive the concept of a dual hyponome system, with two hyponome openings on either side of the ventral rostrum. This concept was originally proposed by Schmidt (1930) and Frentzen (1937) where jetting could take place from any direction and even promote forward horizontal swimming. There is currently no fossil evidence for this, or any hyponome for that matter (Klug and Lehmann 2015), aside from possible imprints (Summesberger et al. 1999; Landman and Cobban 2007). The lateral sinuses of baculitid shells have been interpreted by Klug et al. (2012) to house large eyes, in contrast to accommodating hypothetical dual hyponomes. The curved ventral rostrum of the baculitid, *Sciponoceras*, has been suggested to allow it to

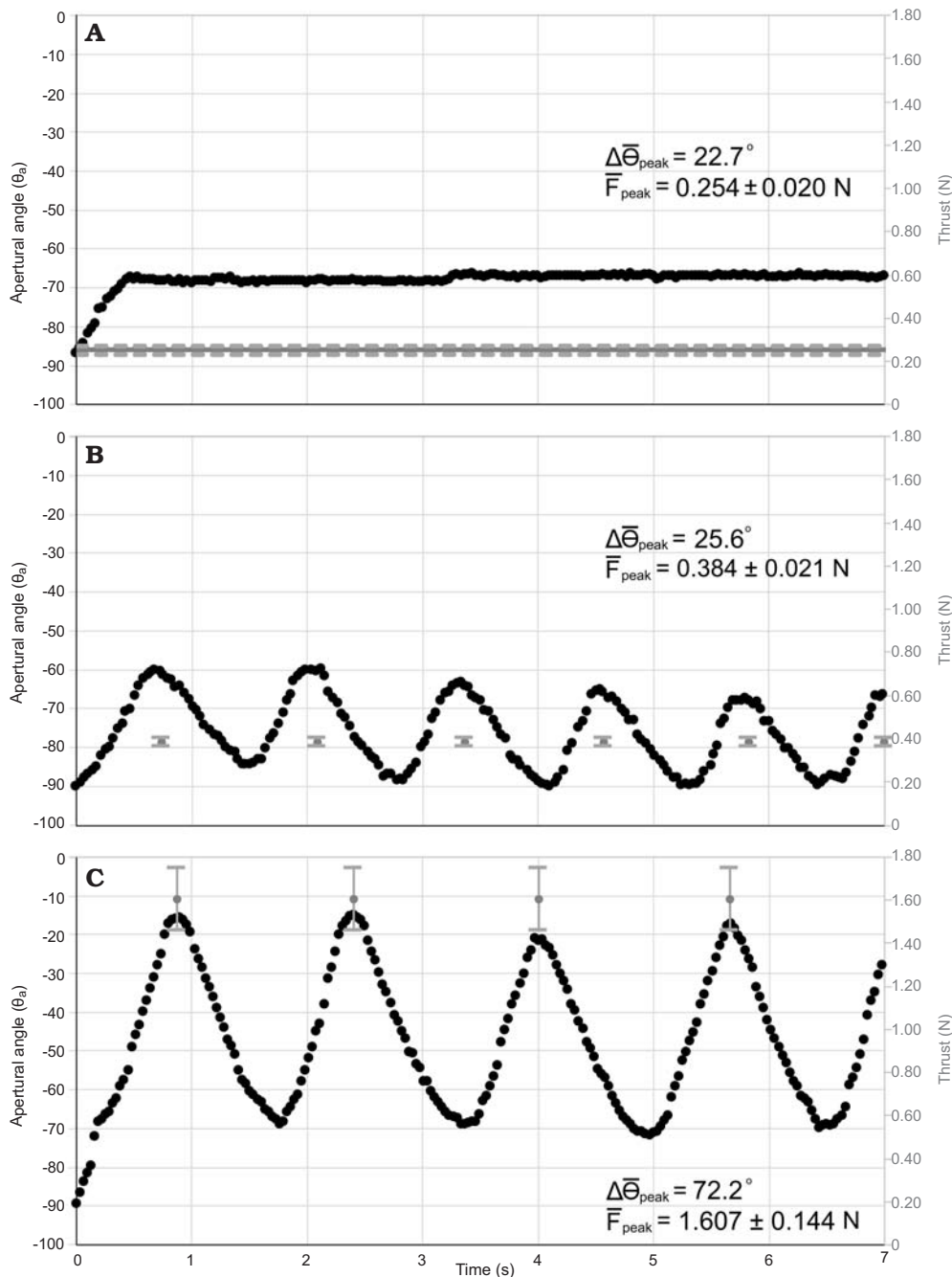


Fig. 11. Thrust required to change the *Baculites compressus* model orientation ( $\theta_a$ ). **A.** Thrust Scenario 1: A continuous thrust supplied to the venter with a similar thrust ratio to *Nautilus* (Table 1). The average change from a vertical resting orientation ( $\Delta \bar{\theta}_{\text{peak}}$ ) is  $22.7^\circ$ . **B.** Thrust Scenario 2: Periodic pulses from a pump with a simulated mantle cavity of 20% soft body volume of *B. compressus* (Table 1). The average change from a vertical resting orientation ( $\Delta \bar{\theta}_{\text{peak}}$ ) is  $25.6^\circ$ . **C.** Thrust Scenario 3: Periodic pulses from a pump with a thrust ratio between *Sepia officinalis* and *Loligo vulgaris* (Table 1). The average change from a vertical resting orientation ( $\Delta \bar{\theta}_{\text{peak}}$ ) is  $72.2^\circ$ . Average peak thrust ( $\bar{F}_{\text{peak}}$ ) error bars represent one standard deviation calibrated from 30 second intervals of pumping.

occasionally rest on the substrate (Crick 1912; Matsumoto and Obata 1962; Klinger 1980). This behavior or demersal behavior could have been possible as long as the living baculitid conformed to its inferred depth of approximately less than 100 m (Fatherree et al. 1998; Lukeneder et al. 2010; Klug et al. 2012). In a nektic setting, a mostly-vertical syn vivo orientation, as implied by the hydrostatic and hydrodynamic experiments of the current study, would rule out the

need for the application of thrust from the ventral direction. Therefore, the ventral rostrum of baculitid shells may not have been a hindrance.

The influence of conch compression and depression in the baculitids were not investigated in the current study. However, the laterally compressed forms such as *B. compressus* appear to be more streamlined than baculitids with ovate whorl sections. This interpretation has led to the de-

piction of such compressed forms as having enhanced lateral mobility (Tsujita and Westermann 1998). During the hydrodynamic restoration of the baculite model (Fig. 9C), movement was preferred in the ventral direction after being rotated in the dorsal direction. This preference is due to a much lower hydrodynamic drag (proportionate to cross sectional area) in the dorso-ventral directions relative to the lateral directions in a compressed form. It is therefore possible that lateral compression of the conch was an adaptation to prevent rolling in the longitudinal axis rather than true streamlining. Orthoconic morphotypes with different whorl section geometries should be comparatively investigated in future studies.

The growth direction and orientation of a stalked cirripede attached to the venter of *Sciponoceras* was interpreted by Hauschke et al. (2011) to have occurred in a setting where the living baculitid moved forward in a more or less horizontal orientation. This idea conflicts with the vertical hydrostatic syn vivo orientations and hydrodynamic capabilities of the baculitid modeled in the current study. Both *Sciponoceras* and *Baculites compressus* probably had similar stability indices based on their similar body chamber lengths (33%; Klug et al. 2012) and degree of shell taper. The position of the adult cirripede on the venter of the shell and the adapical end of the body chamber could have contributed to the total mass distribution toward the apex and venter. A significant change in orientation has been observed for other taxa with epibionts as indicated by changes in the growth of the cephalopod shell (Seilacher and Gishlick 2015). The magnitude of this influence is unknown, however, and would have been less significant during the juvenile stage of the cirripede, when it would have chosen this preferred growth orientation. This specimen reported by Hauschke et al. (2011) is largely enigmatic and warrants further investigation on the baculitid mode of life. It is unknown whether this cirripede orientation is anomalous, or if frequent vertical movement of the *Sciponoceras* could have facilitated this epizoan behavior.

The results of this study suggest that baculitids and similar orthocones assumed a mode of life with very poor mobility in the horizontal directions and rather moderate mobility in the vertical direction, living as a quasiplanktic to nektic vertical migrant (Westermann 1996). Anatomical interpretations of well-preserved specimens support a planktotrophic habit (Kruta et al. 2011; Klug et al. 2012), and oxygen isotope values of aragonitic shells infer the occupation of relatively shallow waters of less than 100 m (Fatherree et al. 1998; Lukeneder et al. 2010; Landman and Klfak 2012; Henderson and Price 2012; Lukeneder 2015; Sessa et al. 2015; Landman et al. 2018). Furthermore, these baculitids were somewhat sedentary and probably lived most of their lives at or near a single location within a few meters from the seafloor (Landman et al. 2018). The constraints imposed on their life habits agree well with their hydrostatic limitations revealed in the current study. Poor horizontal mobility would preclude extensive lateral migration, in con-

trast to the portrayal of seemingly streamlined forms (such as *B. compressus*) as swift, mid-water swimmers (Tsujita and Westermann 1998). The hydrostatic and hydrodynamic properties of the baculitids support a lower energy mode of life in a vertical or near vertical condition.

## Conclusions

Baculitids and other orthocones had the capacity for neutral buoyancy providing that they had sufficient body chamber ratios. The *Baculites compressus* models in the current study demonstrate that orthocones of the mesodome category of body chamber length (Westermann 2013) are neutrally buoyant (or nearly so) and that body chamber lengths of greater than approximately 40% with the modeled geometries will be negatively buoyant. Each of these models exhibit a highly stable, vertical syn vivo orientation in a static setting. These hydrostatic conditions occur in orthoconic cephalopods because they most efficiently separate the total center of mass away from the total center of buoyancy in a linear fashion; by partitioning the shell in to a largely empty section (the phragmocone) and having a higher concentration of mass at the adoral end of the organism (the soft body).

The distribution of cameral liquid in the phragmocone does not alter the syn vivo orientation. Adapically distributing the cameral liquid in a neutrally buoyant baculite model reduces hydrostatic stability, but cannot be used as a counterweight to permit a non-vertical orientation. A concave dorsum similar to *B. grandis* does not shift the mass distribution ventrally or closer to the center of buoyancy. Such a modification would only rotate the aperture in the dorsal direction. In the modified virtual baculite models (Fig. 6D, E) the concave dorsum results in a 5° rotation of the aperture towards the dorsum in a static setting (see Westermann 2013 for alternative findings).

An even distribution of cameral liquid within the phragmocone of the baculite model yields a hydrostatic stability about an order of magnitude larger than the *N. pompilius* model. This difference in hydrostatic stability and differences in hydrodynamic drag are responsible for fundamentally different modes of hydrodynamic restoration between the two models. The *N. pompilius* model behaves as an underdamped harmonic oscillator that wobbles around its equilibrium position before resting. In contrast, the *B. compressus* model experiences overdamped harmonic motion and more quickly returns to its equilibrium position without oscillating.

The large separation between the centers of mass and buoyancy (high stability) of the baculite models result in large restoring moments after the models were rotated from their equilibrium position. Thrust applied to the venter using a continuous water supply and a similar thrust ratio to *N. pompilius* slightly rotated the model (22.7°). The thrust produced from a finite mantle cavity computed for the scaled *B. compressus* similarly rotated the model at small angles (25.6°). An overestimated value of thrust in between the thrust ratios

of the extant coleoids, *Sepia officinalis* and *Loligo vulgaris* significantly rotated the model (72.2°), but such values are unlikely to be produced from the computed mantle cavity volume. Each of the experimental thrust ratios are based on the maximum propulsive burst, which probably would have been too energetically expensive for usual locomotion. Therefore, active orientations were likely less than 25° from vertical. The results of the current study support the interpretations of baculitids and orthocones with similar hydrostatic properties as having lived a nektonic to quasiplanktonic mode of life with a primarily vertical orientation and mobility.

## Acknowledgements

We very much appreciate the help of Neal Larson (Larson Paleontology, Keystone, USA) with collecting the specimens WSU-1400 and WSU-1401 and Don Clements (North Carolina Museum of Natural Sciences, Raleigh, USA) for donating WSU-1450. Each of these specimens were essential in reconstruction of the baculite models. We also thank Peter Minister (Peter Minister Digital Art, Manchester, England) for providing a digital model of the *Nautilus pompilius* soft body. René Hoffmann (Ruhr-Universität Bochum, Germany) and Takao Ubukata (Kyoto University, Japan) are thanked for their constructive reviews of our manuscript.

## References

- 3DFlow. 2018. *3DF Zephyr*. Free Edition. 3DFlow, <https://www.3dflow.net/3df-zephyr-free/>
- Autodesk Inc. 2017a. *Meshmixer 3.3*. Autodesk Inc., San Rafael.
- Autodesk Inc. 2017b. *Netfabb 2017.3*. Autodesk Inc., San Rafael.
- Anderson, E.J. and Demont, M.E. 2000. The mechanics of locomotion in the squid *Loligo pealei*: locomotory function and unsteady hydrodynamics of the jet and intramantle pressure. *The Journal of Experimental Biology* 203: 2851–2863.
- Batt, R.J. 1989. Ammonite shell morphotype distribution in the Western Interior Greenhorn sea and some paleoecological implications. *Palaios* 4: 32–42.
- Brown, D. 2017. *Tracker 4.11.0*. Open Source Physics, <https://physlets.org/tracker/> [retrieved June 21, 2018]
- Chamberlain, J.A. 1981. Hydromechanical design of fossil cephalopods. In: M.R. House and J.R. Senior (eds.), *The Ammonoidea*, 289–336. Systematics Association, London.
- Chamberlain, J.A. 1990. Jet propulsion of *Nautilus*: a surviving example of early Paleozoic cephalopod locomotor design. *Canadian Journal of Zoology* 68: 806–814.
- Cignoni, P. and Ranzuglia, G. 2014. *MeshLab (Version 1.3.3)*. Visual Computing Lab-ISTI-CNR, Pisa. Available from <http://meshlab.sourceforge.net/>
- Collins, D.H., Ward, P.D., and Westermann, G.E.G. 1980. Function of cameral water in *Nautilus*. *Paleobiology* 6: 168–172.
- Crick, G.C. 1912. On the aperture of a baculite from the Lower Chalk of the Chadstock, Somerset. *Proceedings of the Malacological Society of London* 2: 77–80.
- Cunningham, J.A., Rahman, I.A., Lautenschlager, S., Rayfield, E.J., and Donoghue, P.C. 2014. A virtual world of paleontology. *Trends in Ecology and Evolution* 29: 347–357.
- Denton, E.J. and Gilpin-Brown, J.B. 1961. The buoyancy of the cuttlefish *Sepia officinalis* (L.). *Journal of the Marine Biological Association of the United Kingdom* 41: 319–342.
- Falkingham, P.L. 2012. Acquisition of high resolution three-dimensional models using free, open-source, photogrammetric software. *Palaeontologia Electronica* 15: 1–15.
- Fatherree, J.W., Harries, P.J., and Quinn, T.M. 1998. Oxygen and carbon isotopic “dissection” of *Baculites compressus* (Mollusca: Cephalopoda) from Pierre Shale (Upper Campanian) of South Dakota: implications for paleoenvironmental reconstructions. *Palaios* 13: 376–385.
- Fau, M., Cornette, R., and Houssaye, A. 2016. General Palaeontology, Systematics and Evolution (Vertebrate Palaeontology): Photogrammetry for 3D digitizing bones of mounted skeletons: Potential and limits. *General Palaeontology, Systematics and Evolution (Vertebrate Palaeontology)* 15: 968–977.
- Frentzen, K. 1937. Ontogenie, phylogenie und systematic der Amaltheen des Lias Deta Suedwestdeutschlands. *Abhandlungen der Heidelberger Akademie der Wissenschaften, Mathematisch-naturwissenschaftliche Klasse 1937*: 131–236.
- Greenwald, L. and Ward, P.D. 1987. Buoyancy in *Nautilus*. In: B.W. Saunders and N.H. Landman (eds.), *Nautilus—The Biology and Paleobiology of a Living Fossil*. 547–559. Springer, Dordrecht.
- Hall, J. and Meek, F.V. 1854. Description of new species of fossils, from the Cretaceous formations of Nebraska, with observations upon *Baculites ovatus* and *B. compressus*, and the progressive development of the septa in *Baculites*, *Ammonites* and *Scaphites*. *Memoirs of the American Academy of Arts and Sciences New Series* 5 (2): 379–411.
- Hauschke, N., Schöllmann, L., and Keupp, H. 2011. Oriented attachment of a stalked cirripede on an orthoconic heteromorph ammonite—implications for the swimming position of the latter. *Neues Jahrbuch für Geologie und Paläontologie Abhandlungen* 202: 199–212.
- Henderson, R.A. and Price, G.D. 2012. Paleoenvironment and paleoecology inferred from oxygen and carbon isotopes of subtropical mollusks from the late Cretaceous (Cenomanian) of Bathurst Island, Australia. *Palaios* 27 (9): 617–626.
- Hoffmann, R. and Keupp, H. 2015. Ammonoid Paleopathology. In: C. Klug, D. Korn, K. De Baets, I. Kruta, and R.H. Mapes (eds.), *Ammonoid Paleobiology. Volume 1: From Anatomy to Ecology*. *Topics in Geobiology* 43: 876–926.
- Hoffmann, R. and Zachow, S. 2011. Non-invasive approach to shed new light on the buoyancy business of chambered cephalopods (Mollusca). *Proceedings of the International Association for Mathematical Geosciences, Salzburg 2011* [published online, <https://doi.org/10.5242/iang.2011.0163>]
- Hoffmann, R., Lemanis, R., Falkenberg, J., Schneider, S., Wesendonk, H., and Zachow, S. 2018. Integrating 2D and 3D shell morphology to disentangle the paleobiology of ammonoids: a virtual approach. *Palaeontology* 61: 89–104.
- Hoffmann, R., Lemanis, R., Naglik, C., and Klug, C. 2015. Ammonoid Buoyancy. In: C. Klug, D. Korn, K. De Baets, I. Kruta, and R.H. Mapes (eds.), *Ammonoid Paleobiology. Volume I: From Anatomy to Ecology*. *Topics in Geobiology* 43: 611–648.
- Hoffmann, R., Schultz, J.A., Schellhorn, R., Rybacki, E., Keupp, H., Gerden, S.R., Lemanis, R., and Zachow, S. 2014. Non-invasive imaging methods applied to neo- and paleo-ontological cephalopod research. *Biogeosciences* 11: 2721–2739.
- Inoue, S. and Kondo, S. 2016. Suture pattern formation in ammonites and the unknown rear mantle structure. *Scientific Reports* 6: 33689.
- Jacobs, D.K. and Landman, N.H. 1993. *Nautilus*—a poor model for the function and behavior of ammonoids? *Lethaia* 26: 101–111.
- Keupp, H., Röper, M., and Seilacher, A. 1999. Paläobiologische Aspekte von syn vivo-besiedelten Ammonoideen im Plattenkalk des Ober-Kimmeridgiums von Brunn in Ostbayern. *Berliner Geowissenschaftliche Abhandlungen Reihe E Palaeobiologie* 30: 121–145.
- Klinger, H.C. 1980. Speculations on buoyancy control and ecology in some heteromorph ammonites. In: M.R. House and J.R. Senior (eds.), *The Ammonoidea. Systematics Association Special Volume* 18: 337–355. Academic Press, London.
- Klug, C. and Hoffmann, R. 2015. Ammonoid septa and sutures. In: C. Klug, D. Korn, K. De Baets, I. Kruta, and R.H. Mapes (eds.), Am-

- monoid Paleobiology. Volume I: From Anatomy to Ecology. *Topics in Geobiology* 43: 45–90.
- Klug, C. and Lehmann, J. 2015. Soft part anatomy of ammonoids: reconstructing the animal based on exceptionally preserved specimens and actualistic comparisons. In: C. Klug, D. Korn, K. De Baets, I. Kruta, and R.H. Mapes (eds.), *Ammonoid Paleobiology. Volume I: From Anatomy to Ecology. Topics in Geobiology* 43: 515–538.
- Klug, C., Riegraf, W., and Lehmann, J. 2012. Soft-part preservation in heteromorph ammonites from the Cenomanian–Turonian Boundary Event (OAE 2) in the Teutoburger Wald (Germany). *Palaeontology* 55: 1307–1331.
- Knauss, M.J. and Yacobucci, M.M. 2014. Geographic Information Systems technology as a morphometric tool for quantifying morphological variation in an ammonoid clade. *Palaeontologia Electronica* 17 (1): 19A.
- Kröger, B. 2002. On the efficiency of the buoyancy apparatus in ammonoids: evidences from sublethal shell injuries. *Lethaia* 35: 61–70.
- Kruta, I., Landman, N., Rouget, I., Cecca, F., and Tafforeau, P. 2011. The role of ammonites in the Mesozoic marine food web revealed by jaw preservation. *Science* 331: 70–72.
- Kruta, I., Rouget, I., Landman, N.H., Tanabe, K., and Cecca, F. 2009. Aptychus microstructure in Late Cretaceous Ancyloceratina (Ammonoidea). *Lethaia* 42: 312–321.
- Landman, N.H. and Cobban, W.A. 2007. Ammonite touch marks in upper Cretaceous (Cenomanian–Santonian) deposits of the western interior sea. In: N.H. Landman, R.A. Davis, and R.H. Mapes (eds.), *Cephalopods Present and Past: New Insights and Fresh Perspectives*, 396–422. Springer, Dordrecht.
- Landman, N.H., and Klofak, S.M. 2012. Anatomy of a concretion: life, death, and burial in the Western Interior Seaway. *Palaios* 27: 672–693.
- Landman, N.H., Cochran, J.K., Slovacek, M., Larson, N.L., Garb, M.P., Brezina, J., and Witts, J.D. 2018. Isotope sclerochronology of ammonites (*Baculites compressus*) from methane seep and non-seep sites in the Late Cretaceous Western Interior Seaway, USA: Implications for ammonite habitat and mode of life. *American Journal of Science* 318: 603–639.
- Lemanis, R., Korn, D., Zachow, S., Rybacki, E., and Hoffmann, R. 2016. The evolution and development of cephalopod chambers and their shape. *PLoS ONE* 11: 1–21.
- Lemanis, R., Zachow, S., Fusses, F., and Hoffmann, R. 2015. A new approach using high-resolution computed tomography to test the buoyant properties of chambered cephalopod shells. *Paleobiology* 41: 313–329.
- Lukeneder, A. 2015. Ammonoid habitats and life history. In: C. Klug, D. Korn, K. De Baets, I. Kruta, and R.H. Mapes (eds.), *Ammonoid Paleobiology. Volume I: From Anatomy to Ecology. Topics in Geobiology* 43: 689–791.
- Lukeneder, A., Harzhauser, M., Müllegger, S., and Piller, W.E. 2010. Ontogeny and habitat change in Mesozoic cephalopods revealed by stable isotopes ( $\delta^{18}\text{O}$ ,  $\delta^{13}\text{C}$ ). *Earth and Planetary Science* 296: 103–114.
- Matsumoto, T. and Obata, I. 1962. Notes on baculites facies. *Kaseki* 3: 57–63.
- Mironenko, A.A. 2018. Endocerids: suspension feeding nautiloids? *Historical Biology* [published online, <https://doi.org/10.1080/08912963.2018.1491565>]
- Moseley, H. 1838. On the geometrical form of turbinated and discoid shells. *Philosophical Transactions of the Royal Society* 1838: 351–370.
- Naglik, C., Monnet, C., Goetz, S., Kolb, C., De Baets, K., Tajika, A., and Klug, C. 2015a. Growth trajectories of some major ammonoid subclades revealed by serial grinding tomography data. *Lethaia* 48: 29–46.
- Naglik, C., Rikhtegar, F., and Klug, C. 2016. Buoyancy of some Palaeozoic ammonoids and their hydrostatic properties based on empirical 3D models. *Lethaia* 49: 3–12.
- Naglik, C., Tajika, A., Chamberlain, J., and Klug, C. 2015b. Ammonoid locomotion. In: C. Klug, D. Korn, K. De Baets, I. Kruta, and R.H. Mapes (eds.), *Ammonoid Paleobiology. Volume I: From Anatomy to Ecology. Topics in Geobiology* 43: 649–688.
- Neil, T. and Askew, G.N. 2018. Swimming mechanics and propulsive efficiency in the chambered nautilus. *Royal Society Open Science* 5: 170467.
- Okamoto, T. 1996. Theoretical modeling of ammonoid morphology. In: N.H. Landman, K. Tanabe, and R.A. Davis (eds.), *Ammonoid Paleobiology. Topics in Geobiology* 13: 225–251. Plenum, New York.
- Parent, H., Westermann, G.E.G., and Chamberlain, J.A. Jr. 2014. Ammonite aptychi: functions and role in propulsion. *Geobios* 47: 45–55.
- Peterman, D.J. and Barton, C.C. 2017. *Baculite 3D Modeling: A New Method for Computing Buoyancy, Stability, and Orientation with Implications for Ectocochleate Cephalopod Hydrostatics*. Abstract PP11D-1063 presented at 2017 Falling Meeting, AGU, New Orleans, Louisiana.
- Peterman, D.J. and Barton, C.C. 2019. Power scaling of ammonitic suture patterns from Cretaceous Ancyloceratina: constraints on septal/sutural complexity. *Lethaia* 52: 77–90.
- Peterman, D.J. and Ciampaglio, C.N. 2018. How stable were orthoconic cephalopods? Hydrodynamic analyses of restoring moments from neutrally buoyant, 3D printed models of ectocochleate cephalopods. *Geological Society of America Annual Meeting in Indianapolis, Abstracts with Programs* 50: 6.
- Peterman, D.J., Barton, C.C., and Yacobucci, M.M. 2019. The hydrostatics of Paleozoic ectocochleate cephalopods (Nautiloidea and Endoceratoidea) with implications for modes of life and early colonization of the pelagic zone. *Palaeontologia Electronica* [published online, <https://doi.org/10.26879/884>]
- Peterman, D.J., Ciampaglio, C.N., and Barton, C.C. 2018. The hydrostatics of Paleozoic orthoconic cephalopods (Nautiloidea) with implications for early colonization of the pelagic zone. *Geological Society of America Annual Meeting in Indianapolis, Abstracts with Programs* 50: 4.
- Petti, F.M., Avanzini, M., Belvedere, M., De Gasperi, M., Ferretti, P., Girardi, S., Remondino, F., and Tomasoni, R. 2008. Digital 3D modelling of dinosaur footprints by photogrammetry and laser scanning techniques: integrated approach at the Coste dell'Anglone tracksite (Lower Jurassic, southern Alps, northern Italy). *Studi Trentini di Scienze Naturali Acta Geologica* 83: 303–315.
- Raup, D.M. 1967. Geometric analysis of shell coiling: coiling in ammonoids. *Journal of Paleontology* 41: 43–65.
- Raup, D.M. and Chamberlain, J.A. 1967. Equations for volume and center of gravity in ammonoid shells. *Journal of Paleontology* 41: 566–574.
- Reyment, R.A. 1958. Some factors in the distribution of fossil cephalopods. *Stockholm Contributions in Geology* 1: 97–184.
- Reyment, R.A. 1973. Factors in the distribution of fossil cephalopods; Part 3, Experiments with exact models of certain shell types. *Bulletin of the Geological Institutions of the University of Uppsala, New Series* 4 2: 7–41.
- Say, T. 1820. Observations on some species of zoophytes, shells, etc. principally fossil. *American Journal of Science* 2: 34–45.
- Saunders, W.B. and Shapiro, E.A. 1986. Calculation and simulation of ammonoid hydrostatics. *Paleobiology* 12: 64–79.
- Schmidt, H. 1930. Ueber die Bewegungsweise der Schalencephalopoden. *Palaeontologische Zeitschrift* 12: 194–208.
- Seilacher, A. and Gishlick, A.D. 2015. *Morphodynamics*. 531 pp. CRC Press Taylor & Francis Group, Boca Raton, Florida.
- Seilacher, A. and Keupp, H. 2000. Wie sind Ammoniten geschwommen? *Fossilien* 2000: 310–313.
- Sessa, J.A., Larina, E., Knoll, K., Garb, M., Cochran, J.K., Huber, B.T., MacLeod, K.G., and Landman, N.H. 2015. Ammonite habitat revealed via isotopic composition and comparisons with co-occurring benthic and planktonic organisms. *Proceedings of the National Academy of Sciences of the United States of America* 112: 15562–15567.
- Sessa, J.A., Ferguson, K., Landman, N.H., and MacLeod, K.G. 2018. Using isotopic composition to determine growth and ecology in baculite and scaphite ammonites. *Geological Society of America Abstracts with Programs* 50 (6) [published online, <https://doi.org/10.1130/abs/2018AM-319800>]
- Shigeta, Y. 1993. Post-hatching early life history of Cretaceous Ammonoidea. *Lethaia* 26: 133–146.
- Summesberger H., Jurkovek, B., and Kolar-Jurkovek, T. 1999. Roll-

- marks of soft parts and possible crop content of Late Cretaceous ammonites from the Slovenian karst. In: F. Olóriz and F.J. Rodríguez-Tovar (eds.), *Advancing Research on Living and Fossil Cephalopods*, 335–344. Kluwer Academic, New York.
- Sutton, M.D., Rahman, I.A., and Garwood, R.J. 2014. *Techniques for Virtual Palaeontology*. 208 pp. John Wiley & Sons Inc., Chichester.
- Tajika, A., Morimoto, N., Wani, R., Naglik, C., and Klug, C. 2015a. Intraspecific variation of phragmocone chamber volumes throughout ontogeny in the modern nautilid *Nautilus* and the Jurassic ammonite *Normannites*. *PeerJ* 3: 1–28.
- Tajika, A., Naglik, C., Morimoto, N., Pascual-Cebrian, E., Hennhöfer, D.K., and Klug, C. 2015b. Empirical 3D-model of the conch of the Middle Jurassic ammonite microconch *Normannites*, its buoyancy, the physical effects of its mature modifications and speculations on their function. *Historical Biology* 27: 181–191.
- Tanabe, K., Shigeta, Y., and Mapes, R.H. 1995. Early life history of Carboniferous ammonoids inferred from analysis of fossil assemblages and shell hydrostatics. *Palaios* 10: 80–86.
- Teichert, C. 1964. Morphology of hard parts. In: R.C. Moore (ed.), *Treatise on Invertebrate Paleontology Part K Mollusca* 3, K12–K53. Geological Society of America, Boulder, and University of Kansas Press, Lawrence.
- Thompson, J.T. and Kier, W.M. 2002. Ontogeny of squid mantle function: changes in the mechanics of escape-jet locomotion in the oval squid, *Sepioteuthis lessoniana* Lesson, 1830. *Biological Bulletin* 203: 14–26.
- Trueman, A.E. 1941. The ammonite body-chamber, with special reference to the buoyancy and mode of life of the living ammonite. *Quarterly Journal of the Geological Society* 384: 339–383.
- Tsujita, C.J. and Westermann, G.E.G. 1998. Ammonoid habitats and habits in the Western Interior Seaway: a case study from the Upper Cretaceous Bearpaw Formation of southern Alberta, Canada. *Palaeogeography, Palaeoclimatology, Palaeoecology* 144: 135–160.
- Ward, P.D. 1976. *Stratigraphy, Paleocology and Functional Morphology of Heteromorph Ammonites of the Upper Cretaceous Nanaimo Group, British Columbia and Washington*. 191 pp. Unpublished Ph.D. dissertation, McMaster University, Department of Geology, Hamilton.
- Ward, P.D. 1979. Cameral liquid in *Nautilus* and ammonites. *Paleobiology* 5: 40–49.
- Ward, P.D. 1987. *The Natural History of Nautilus*. 267 pp. Allen and Unwin, Boston.
- Westermann, G.E.G. 1977. Form and function of orthocone cephalopod shells with concave septa. *Paleobiology* 3: 300–321.
- Westermann, G.E.G. 1996. Ammonoid life and habitat. In: N.H. Landman, K. Tanabe, and R.A. Davis (eds.), *Ammonoid Paleobiology*, 607–707. Plenum, New York.
- Westermann, G.E.G. 2013. Hydrostatics, propulsion and life-habits of the Cretaceous ammonoid *Baculites*. *Revue de Paléobiologie* 32: 249–265.